OSCILLATION MONITORING SYSTEM BASED ON

WIDE AREA PHASOR MEASUREMENTS IN POWER SYSTEMS

By

GUOPING LIU

A dissertation submitted in partial fulfillment of
the requirements for the degree of

DOCTOR OF PHILOSOPHY

WASHINGTON STATE UNIVERSITY
School of Electrical Engineering and Computer Science

AUGUST 2010

To the Faculty of Washington State University:

The members of the Committee appointed to examine the dissertation of GUOPING LIU find it satisfactory and recommend that it be accepted.

_____

Vaithianathan Venkatasubramanian, Ph.D, Chair

_____

Anjan Bose, Ph.D

_____

Kevin Tomsovic, Ph.D

ACKNOWLEDGMENT

I would like to express my sincere gratitude to my advisor Professor Vaithianathan Venkatasubramanian for his guidance, enlightening instruction and support throughout my study at Washington State University.

I wish to thank Professor Anjan Bose and Professor Kevin Tomsovic for their instruction and valuable discussions on this work. I also want to say thanks to all the other professors who have helped me during my studies at Washington State University.

I am grateful to Ritchie Carroll and his group in Tennessee Valley Authority (TVA), who designed the real-time environment for the Oscillation Monitoring System. William A. Mittelstadt, James Burns et al from Bonneville Power Administration provide valuable help and guidance to this work. I also appreciate the help from Xunning Yue, Qiang Zhang and Junling Li in the implementation stage of the system.

This research has been supported by funding from several agencies including Power System Engineering Research Center (PSERC), Tennessee Valley Authority (TVA), Entergy, Bonneville Power Administration (BPA), US Department of Energy, and Consortium for Electric Reliability Technology Solutions (CERTS).

Finally, I wish to thank my parents and my wife for their encouragement and enduring love.

OSCILLATION MONITORING SYSTEM BASED ON

WIDE AREA PHASOR MEASUREMENTS IN POWER SYSTEMS

Abstract

by Guoping Liu, Ph.D.
Washington State University
August 2010

Chair: Mani V. Venkatasubramanian

This dissertation presents an Oscillation Monitoring System (OMS) based on real-time wide-area measurements from Phasor Measurement Units (PMU). This OMS is designed to detect poorly-damped or negatively-damped electromechanical modes in the early stage of an oscillation event, as well as provide warning signals from normal system operating conditions when mode damping becomes insufficient for safe operation of power systems. Depending on different mathematical models of the measured data, different processing algorithms are used. The system disturbance part of the OMS is designed to monitor system events in real-time for the purpose of emergency control, while the ambient part monitors the system without any disturbances for the purpose of preventive control. These two parts are complementary to each other, constituting a complete monitoring system.

Power system responses following system disturbances contain both linear and nonlinear phenomena. Moreover, presence of noise and switching events in the measurements can upset the accuracy of results. For these reasons, we developed different crosscheck rules to avoid false alarms due to inconsistent estimations. Three signal processing algorithms are used, namely, Prony's Method, Matrix Pencil

Method and Hankel Total Least Squares (HTLS) method. Results from these engines are processed using a custom developed set of rules for handling the complexities of modal analysis from real-time PMU measurements.

Ambient data are collected during normal system operations. Unlike previous methods used for ambient data processing, the modified Frequency Domain Decomposition (FDD) is able to simultaneously identify damping and mode shape of the dominant mode using several minutes of ambient data. FDD also works well for noisy measurements and correlated inputs, and it appears to be useful specifically for analyzing real-time PMU measurements. Together with the post-disturbance data processing following system events, it provides a powerful framework of an oscillation monitoring system from wide-area PMU measurements.

TABLE OF CONTENTS

Page

ACKNOWLEDGEMENTS iii

ABSTRACT iv

LIST OF TABLES ix

LISTOF FIGURES x

CHAPTER ONE: INTRODUCTION 1

CHAPTER TWO: FRAMEWORK OF OSCILLATION MONITORING SYSTEM 7

2.1. Background of Phasor Measurement Technology 7

2.2. Types of Measurement Data 8

2.3. Basic Framework of Oscillation Monitoring System 9

2.3.1 Data Preprocessing 10

2.3.2 Event Detection. 11

2.3.3 Moving Window Analysis and Result Crosschecks 12

CHAPTER THREE: OSCILLATION MONITORING USING SYSTEM DISTURBANCE DATA 16

3.1. Linear Analysis of Power System Small Signal Stability 17

3.2. Engines for Modal Analysis 17

3.2.1 Prony's Method. 18

3.2.2 Matrix Pencil Method. 19

3.2.3 Hankel Total Least Square (HTLS) Method. 22

3.2.4 Comparison of Three Methods 24

3.3. Oscillation Monitoring Following Large Disturbances 26

3.4. Case Studies for Oscillation Monitoring 29

3.4.1 Case I 29

3.4.2 Case II 33

3.4.3 Case III 35

CHAPTER FOUR: OSCILLATION MONITORING USING AMBIENT DATA 37

4.1. Frequency Domain Decomposition 38

4.1.1 Theoretical Background 38

4.1.2 Implementation Issues 44

4.2. Test of Frequency Domain Decomposition on Small Linear Systems 47

4.2.1 Test of FDD for Systems with Different Damping Ratios 47

4.2.2 Test of FDD for Different Data Lengths 52

4.2.3 Some Features of FDD 53

4.2.4 Guard against Underestimates 57

4.3. Test of Frequency Domain Decomposition on Small Power Systems 58

4.4. Case Studies 63

4.4.1 WECC August 10th 1996 Event 63

4.4.2 TVA November 29th 2007 Event 66

4.4.3 WECC August 22nd 2006 Event 68

CHAPTER FIVE: CONCLUSIONS 74

REFERENCES 76

Appendix A 82

Appendix B 84

LIST OF TABLES

TABLE 3.1: COMPARISON OF THREE METHODS UNDER NOISY MEASUREMENTS (30 DB) 25

TABLE 3.2: COMPARISON OF THREE METHODS UNDER NOISY MEASUREMENTS (20 DB)..... 25

TABLE 3.3: AVERAGE TIME NEEDED FOR ONE SIMULATION RUN..... 26

TABLE 4.1: TEST OF FDD ON 100 DIFFERENT SYSTEMS..... 51

TABLE 4.2: EFFECT OF DATA LENGTH ON THE RESULTS OF FDD (2% DAMPING RATIO)..... 53

TABLE 4.3: EFFECT OF DATA LENGTH ON THE RESULTS OF FDD (5% DAMPING RATIO) 53

TABLE 4.4: EFFECT OF DATA LENGTH ON THE RESULTS OF FDD (10% DAMPING RATIO) 53

TABLE 4.5: EFFECT OF MEASUREMENT NOISE ON FDD (2% DAMPING RATIO) 54

TABLE 4.6: EFFECT OF CORRELATED INPUTS ON THE RESULTS OF FDD
(2% DAMPING RATIO) 56

TABLE 4.7: SYSTEM CONDITIONS FOR THREE TEST CASES..... 59

TABLE 4.8: RESULTS BY FDD FOR THREE TEST CASES USING 5 MINUTES GENERATOR
ANGLE DATA..... 59

TABLE 4.9: IDENTIFIED MODES FROM FDD ON AUGUST 10TH, 1996..... 65

TABLE 4.10: RESULTS OF PRONY ANALYSIS FOR THE BRAKE TESTS ON AUG 22ND 2006 69

TABLE 4.11: RESULTS OF DIFFERENT METHODS ON AMBIENT AND PROBING TEST
DATA ON AUG 22ND 2006 71

LIST OF FIGURES

Fig. 2.1. Simplified flowchart for the Oscillation Monitoring System 10

Fig. 2.2. Flowchart for event detection in the Oscillation Monitoring System 12

Fig. 3.1. One line diagram of two-area system 27

Fig. 3.2. Active powers of line 7-8 circuit #2 following a 0.1 sec three phase line fault 28

Fig. 3.3. Frequency and damping ratio estimates following a 0.1 sec three phase line fault 28

Fig. 3.4. The voltage magnitude at Malin in Aug. 4, 2000 30

Fig. 3.5. Frequency and damping ratio estimates at Grand Coulee for Case I 31

Fig. 3.6. Frequency and damping ratio estimates at Malin Substation for case I 31

Fig. 3.7. Frequency and damping ratio estimates at Devers (SCE1) for case I 31

Fig. 3.8. Consistent local estimates in all PMUs for case I 32

Fig. 3.9. Frequency and damping ratio estimates of inter-area oscillation detection for case I 33

Fig. 3.10. The voltage magnitude at PMU 3 for case II 34

Fig. 3.11. Consistent local estimates in all PMUs for case II 34

Fig. 3.12. Frequency and damping ratio estimates at PMU 3 for Case II 35

Fig. 3.13. Frequency and damping ratio estimates of inter-area oscillation detection for Case II 35

Fig. 3.14. The voltage magnitude at PMU 1 for case III 36

Fig. 3.15. Frequency and damping ratio estimates of PMU 1 for Case III 36

Fig. 4.1. Complex Mode Indication Function (CMIF) for a poorly damped linear system 48

Fig. 4.2. Pole estimates by FDD for a poorly damped LTI system 49

Fig. 4.3. Pole estimates by FDD for a medium damped LTI system 50

Fig. 4.4. Mode estimates by FDD for a well damped LTI system 50

Fig. 4.5. Mode shape identified by FDD for the LTI system 55

Fig. 4.6. Rotated mode shape identified by FDD for the LTI system 55

Fig. 4.7. Time domain convolution when singular values less than one half of the peak value are truncated 58
Fig. 4.8. Time domain convolution when singular values less than 1/5 of the peak value are truncated 58
Fig. 4.9. Mode shape estimated by FDD in the two-area system for Case I 61
Fig. 4.10. Mode shape estimated by FDD in the two-area system for Case III 61
Fig. 4.11. Means and standard deviations of frequency and damping ratio estimates by FDD and YW for all three cases 63
Fig. 4.12. Means and standard deviations of frequency and damping ratio estimates by FDD and N4SID for all three cases 63
Fig. 4.13. Active power in the tie-line from Malin to Round Mountain line #1 during Aug 10th 1996 blackout 64
Fig. 4.14. Voltage angle at Cumberland Substation on November 29th, 2007 66
Fig. 4.15. Identified mode shape by prony analysis on Nov 29th 2007 in TVA 67
Fig. 4.16. Identified mode shape by FDD on Nov 29th 2007 in TVA 68
Fig. 4.17. Mode shape of the 0.24 Hz mode by Matrix Pencil Method during the first Chief Joseph Brake test on August 22nd, 2006 69
Fig. 4.18. Mode shape of the 0.37 Hz mode by Matrix Pencil Method during the first Chief Joseph Brake test on August 22nd, 2006 70
Fig. 4.19. Identified mode shape by FDD before the first brake test on August 22nd 2006 71
Fig. 4.20. Identified mode shape by FDD after the probing test on August 22nd 2006 72
Fig. 4.21. Identified mode shape by FDD during noise probing test on August 22nd 2006 (0.24 Hz mode) 73
Fig. 4.22. Identified mode shape by FDD during noise probing test on August 22nd 2006 (0.37 Hz mode) 73

Dedication

This dissertation is dedicated to my parents and my wife.

CHAPTER ONE

INTRODUCTION

Small signal stability problem of power systems has remained a concern for power engineers for the past several decades. With growing loads, the power transfers over long geographical distances among different power companies have been increasing steadily. However, these power transfers are limited by low frequency electromechanical oscillations in many power systems all over the world. In the system of the Western Electricity Coordinating Council (WECC) in the US for example, the threat of low-frequency oscillations is a persistent concern in summer when a large amount of power is transmitted from the hydro-power abundant region in the Pacific Northwest to the load centers in the southwest. When the power transfer is high, the damping of the oscillatory inter-area modes can decrease accordingly, and the resulting insufficient damping can lead to growing oscillations as seen during the Aug 10^{th} blackout in 1996 [1], [2]. Such inter-area oscillations, as well as local oscillations involving only one or several generators, are concerns for operational reliability of power systems.

Traditionally, modal analysis is the most widely used offline method to analyze oscillatory stability of power systems. This method needs to linearize the Differential-Algebraic Equation (DAE) model of a power system around an equivalent point and then calculate the eigenvalues of the linearized system matrix [3]. Thus the result from each modal analysis is valid for only one operating point. For a real power system, its operating point keeps changing due to changes in load pattern and system topology. Furthermore, power transfers among power companies have become more and more unpredictable in recent years because of market deregulation, making it more difficult to predict actual system behaviors based on modal analysis for limited number of system conditions.

Moreover, modal analysis is based on modeling of individual components in the system, e.g. generators, exciters etc. The model and model parameters can be obtained from field tests, either by the manufacturer before the commissioning of the device or by the utilities afterwards. For a large system, modeling the dynamics of all the devices is a daunting task if not impossible. Even for the devices which have had field tests, inaccurate model and model parameters are still not uncommon. This is the main reason why system behaviors are not well captured in some cases, e.g. the WECC blackout in August 10^{th} 1996[1].

Due to these limitations of offline modal analysis, there has been increasing interest in measurement-based methods in recent years. All over the world, efforts are underway to use synchrophasor measurement-based information networks to bring the Phasor Measurement Units (PMU) measurements into the control center from different parts of a large power system to determine the current state of the system [4]. These networks are called Wide Area Measurement Systems (WAMS). In WAMS, the data from the PMUs are tagged with an accurate time stamp from satellites and sent to Phasor Data Concentrators (PDC) located in control centers through digital communication channels. These measurements from the whole power system are synchronized in time. The synchronized view of the system, as well as the angle information available from PMUs, provides great potential for many applications in power systems. For example, PMU measurements can be used to improve state estimation, both in speed and robustness. Wide area monitoring and control based on PMU measurements has shown great potential in problems such as transient stability, small signal stability and voltage stability. In this dissertation, we present a complete Oscillation Monitoring System (OMS) based on real-time wide-area measurements from PMUs. This OMS is designed to detect poorly-damped or negatively-damped electromechanical modes in the early stage of an oscillation event, as well as provide warning signals from normal system operating conditions when mode damping becomes insufficient for safe operation of power systems. Then, we can initiate

appropriate controls to damp out the oscillations before they become critical.

PMU measurements can be categorized into three different types. Each type of these measurements has its own mathematical model and processing algorithms. The *system disturbance type* data are the measurements immediately after small or large disturbances to the system, including generator outage, transmission line tripping etc. System response following a small disturbance is linear, in the form of a sum of exponential terms [3]. It can be processed by prony analysis, which includes Prony's Method, Matrix Pencil Method, Hankel Total Least Squares (HTLS) method etc [5], [6]. System response following a large disturbance is more complicated because nonlinearities play an important role in the measured data, especially in the first few cycles after the disturbance. There are algorithms from nonlinear system theory to deal with these nonlinearities, such as Hilbert Transformation [7]. In our proposed Oscillation Monitoring System, prony analysis is combined with moving window analysis and crosscheck rules to deal with these nonlinearity factors [6].

The second type is called *ambient type measurements*, which are collected when power system is in normal operating condition without major system disturbances. Most ambient type methods model ambient PMU measurements as outputs from a linear system driven by white noises. The linear system model can be an autoregressive (AR) model [8], [9], an autoregressive moving average (ARMA) model [10] or a Stochastic State Space model [11], [12]. Besides these block-processing algorithms, recursive algorithms also use AR model but their coefficients are updated in a recursive manner. These methods include Kalman filtering technique [13], Least-mean-square (LMS) adaptive filtering [14], robust recursive least square (RRLS) [15], Regularized Robust RLS (R3LS) [16]. RRLS and R3LS are shown to be able to process ambient as well as ringdown measurements following system disturbances. An overview of the above methods is available in [17]. In addition to the algorithms applied to direct measurements, other derived information can be utilized as well. For example, covariance matrices are used for

least square estimation of system matrix in [18]. Generally speaking, all of the methods mentioned above belong to the time domain. In the frequency domain, a simple FFT of real power signals is used in [19], but it provides no damping estimation. The Yule-Walker Spectrum (YWS) method in [20] is basically the same as [9] except that it calculates autocorrelations from Power Spectral Density (PSD) instead of directly from the time domain. The authors in [21] model the phase angle difference as the output of a second order system driven by random step changes. However, the measurements are needed over a rather long time-window for damping estimation, and this restricts options for initiating any preventive control.

The third type of data is measured from *direct dynamic tests* of the system, including brake tests, single mode probing tests and noise probing tests. The brake tests and single mode probing tests are essentially the same as system disturbances and can be processed by prony analysis. If both input and output measurements from noise probing tests are used, it is a problem of system identification. Methods such as Subspace State Space System Identification (N4SID) [11], [12], [22] can be used to identify critical system modes. If only outputs from noise probing testes are processed, the problem is basically the same as the ambient condition except that the noise probing signal has larger impact than the random load variation across the system.

Besides mode frequency and damping, mode shape is also important information in understanding and controlling a specific mode. Mode shape can be obtained from offline model analysis [3] or prony analysis of measured data after system disturbances [5], [6]. Recent research has focused on estimating mode shape from ambient PMU measurements. In [23], magnitudes of a mode shape are given by relative magnitude of Power Spectrum Density of each measured channel and phases of the mode shape are given by relative angle of Cross Spectrum Density (CSD). In [24], mode shape is calculated by curve fitting on the ratio of CSD and PSD. Authors in [25] further demonstrate that mode shape is actually a transfer function between

state variables evaluated at that mode. This transfer function can be identified by Channel Matching Method in [26] or by a least square ARX model in [25]. The accuracy of the above mode shape estimations depends on not only the identified transfer function, but also the accuracy of the estimated mode. Moreover, no damping can be estimated at the same time.

In this dissertation, we present an Oscillation Monitoring System that monitors frequency, damping and mode shape of dominant electromechanical modes from both ambient and post-disturbance PMU measurements. As discussed in [27], ambient type methods and real-time post-disturbance methods are complementary to each other and should work in parallel to monitor small signal stability of power systems. The ambient type methods are mainly suited for identifying the dominant oscillatory modes for the current system condition. In most cases, problematic oscillations are triggered by some radical changes in the system, and the post-disturbance type methods are more appropriate for identifying sudden changes in the damping of oscillatory modes. In our proposed Oscillation Monitoring System developed at Washington State University (WSU) [28], these two types of methods work in a complementary manner. A prototype version of our OMS has already been implemented into the Phasor Data Concentrator at Tennessee Valley Authority (TVA) [29]. A more detailed description of the proposed OMS is shown in Chapter 2.

Chapter 3 discusses the post-disturbance type methods, and extends the earlier work by Jaime Quintero in his doctoral dissertation [5] at WSU. In this chapter, we summarize our efforts to develop an automatic oscillation monitoring system which is a rule-based expert system that monitors PMU measurements in real time to detect the danger of growing or poorly damped oscillations in the early stages of the event. Three modal analysis methods from signal processing theory are used in this chapter, namely, Prony's Method, Matrix Pencil Method and Hankel Total Least Square (HTLS) method [6]. Section 3.1 provides the common mathematical model for all the algorithms. All these methods try to fit a sum of exponential terms to the uniformly

sampled data. In section 3.2, Prony's method, Matrix Pencil Method and Hankel Total Least Squares (HTLS) are introduced and compared. The application of modal analysis engine following large disturbances is discussed in Section 3.3, followed by actual testing cases from real power system measurements in Section 3.4.

In Chapter 4, we combine prony analysis with the original method of Frequency Domain Decomposition (FDD) [30]-[33] for real time analysis of ambient PMU measurements in power systems. Unlike the previous ambient methods, this modified FDD method is able to simultaneously identify damping and mode shape of the dominant mode using several minutes of ambient data. Section 4.1 presents the theoretical background and some implementation issues for Frequency Domain Decomposition. In Section 4.2, FDD is applied to simple linear systems to illustrate some of its important properties. In Section 4.3, FDD is applied to simulated response of a small power system. Section 4.4 discusses several case studies using real PMU measurements in power systems.

Finally in Chapter 5, we present conclusions for our proposed OMS. Challenging issues and future research trend are also discussed.

CHAPTER TWO

FRAMEWORK OF OSCILLATION MONITORING SYSTEM

In this chapter, we introduce the framework of the proposed Oscillation Monitoring System (OMS). This OMS is able to deal with both system disturbance data and ambient data using different algorithms. The system disturbance part is designed to monitor system events in real-time for the purpose of emergency control, while the ambient part monitors the system without any disturbances for the purpose of preventive control. These two parts are complementary to each other, constituting a complete monitoring system.

This chapter is organized as follows. Section 2.1 introduces the background of phasor measurement technology. Different types of measurements from PMUs are described in Section 2.2. In Section 2.3, we present a complete structure of the proposed OMS.

2.1. Background of Phasor Measurement Technology

A phasor is a short-hand expression for sinusoidal waveforms with a common frequency. For example, a sinusoidal waveform $x(t) = X_m \cos(\omega t + \phi)$ is represented by a phasor $X = X_m / \sqrt{2} e^{j\phi}$, where the phase angle ϕ of the phasor is determined by the starting time (t = 0) of the sinusoid [34]. When the waveform is observed at a constant interval of multiples of the signal period, the observed phasor X is a constant. Otherwise the observed phasor only has constant magnitude with changing phase angles. For a synchrophasor, the instantaneous phase angle is relative to a cosine function at nominal system frequency synchronized to Universal Time Coordinated (UTC). The time source of high accuracy is available from Global Positioning System (GPS).

Phasor Measurement Unit (PMU) is a commercial product of this technology.

Since its birth in the 1990s, PMU has changed the power industry in many ways. Measurements from PMUs are tagged with an accurate time stamp from the satellites and sent to Phasor Data Concentrator (PDC) in the control center, so the measurements from the whole power system can be synchronized in time. The synchronized view of the system, as well as information of phasor angles, provides great potential for many applications including state estimation, wide area monitoring and control etc. System operators equipped with these powerful tools are more efficient in operating power systems safely.

2.2. Types of Measurement Data

PMU measurements can be categorized into three different types according to the nature of the measurements. The system disturbance type data are the measurements immediately after small or large disturbances to the system, including generator outage, transmission line tripping etc. The responses can be in the form of a growing oscillation, a sustained undamped oscillation or a "ringdown", i.e. an oscillation back to the old or new equivalent point. Since the response is mathematically a sum of exponential terms [3] when the disturbance is small, prony analysis is used to analyze this type of data. The methods used for prony analysis in the proposed OMS include Prony's Method, Matrix Pencil Method, Hankel Total Least Squares (HTLS) method [6] etc.

Ambient type data are collected when the system is in a normal operating condition and the only inputs to the system are the random load changes across the entire system. The main advantage of analyzing ambient data is that the ambient type methods work in a non-intrusive manner, so the collection of ambient data is cheap and always available. For this reason, research on ambient type measurements has been a hot topic in recent years. Frequency Domain Decomposition (FDD) [27], subspace identification [11], [12] etc are the methods for this type of data.

The third type of data is measured from direct dynamic tests applied to power

systems. These tests include brake tests, single mode probing tests and noise probing tests. For example, Bonneville Power Administration (BPA) conducts brake tests at Chief Joseph every year to investigate the dynamic performance of the WECC system. However, if the system is small signal unstable, brake tests may lead to growing oscillations and cascading blackouts, thus the tests need to be carefully planned and implemented. Noise probing tests have also been performed by BPA in recent years and they have smaller impacts to the system. Since system dynamic tests are expensive and require a lot of man power, this type of PMU measurements is the rarest among all three categories. From analysis point of view, the brake tests and single mode probing tests are essentially the same as system disturbances. For noise probing tests, the measured outputs are also random, although colored by system dynamics. If both input and output measurements are used, it is a problem of system identification. If only outputs are processed, the problem is basically the same as the ambient condition except that the noise probing signal has larger impact than the random load variation across the system.

2.3. Basic Framework of Oscillation Monitoring System

The complete Oscillation Monitoring System includes both ambient type methods and post-disturbance type methods. A simplified flowchart of the Oscillation Monitoring System is shown in Fig. 2.1. The program periodically reads data from the PDC and preprocess them to deal with issues such as missing channels, bad data etc. Depending on whether any system event is detected in the system, the OMS will choose either ambient or post-disturbance type methods accordingly. If the results from moving window analysis are consistent, the OMS will send an alarm to system operators or trigger damping controllers directly. The event detection part of the OMS is covered in more detail in the later sections in Chapter 2. In Chapter 3, we describe the system-disturbance part of the OMS, and Chapter 4 corresponds to the ambient part of the OMS.

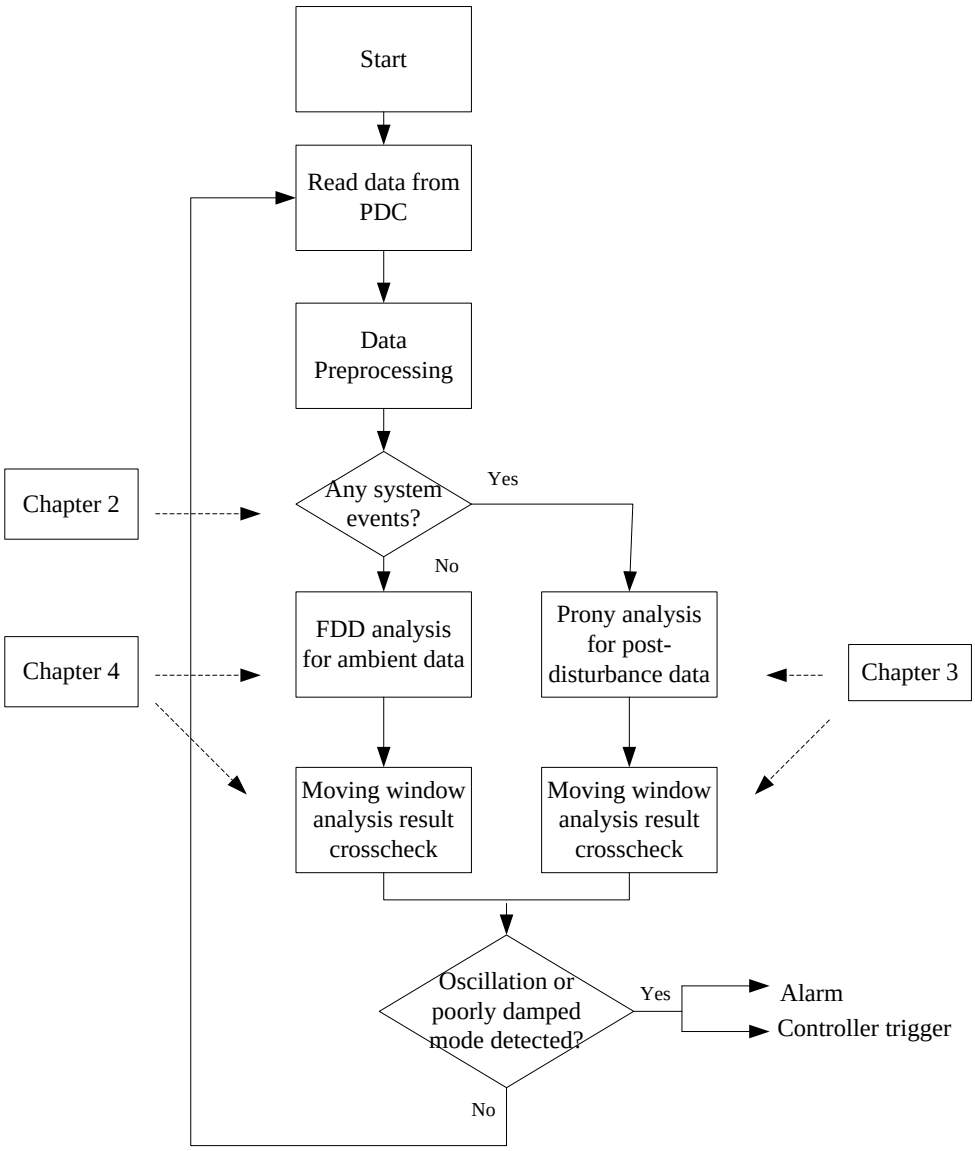

Fig. 2.1. Simplified flowchart for the Oscillation Monitoring System

2.3.1. Data Preprocessing

After data is read from PDC, the first step is to clean up the measurements. It is not uncommon to have bad data in the original data stream, including missing data, missing channels, bad measurements etc. So data preprocessing is an important step to ensure the accuracy of further analysis. A simple criterion is used in the proposed OMS, i.e. if there is a missing data channel, the remaining channels will be used. If there are only a few missing or bad data in a channel, linear interpolation is applied.

However, if there are too many missing or bad data, that channel is simply discarded. The number of bad data that is considered to be ‘too many’ depends on the algorithm used for analysis, and the thresholds of different algorithms are set according to off-line studies based on historical measurements.

2.3.2. Event Detection

The next step after data preprocessing is to detect system events. In the proposed OMS, we use frequency, voltage magnitude and current magnitude for this purpose. The flowchart is shown in Fig. 2.2 as follows. Relative angles between key 500kV buses also contain useful information, and they can be used with care for event detection as well.

From the flowchart in Fig. 2.2, it is seen that three types of calculated values are used for event detection. The maximum and minimum value of frequency measurements are calculated first, which should be in the small range of 59.95~60.05 Hz in normal operating conditions. If the maximum or minimum value is out of the above range, it usually indicates something abnormal in the system. The maximum absolute difference between adjacent samples is used to detect fast changes in the system, e.g. a line fault, or capacitor switching etc. And the standard deviations of voltage and current magnitudes are used mainly for slower events, such as low frequency oscillations. If any of the above tests exceeds pre-defined thresholds, the OMS will set the event flag to be true and proceed to the next step involving actual prony or FDD analysis. The choice of these pre-defined thresholds is in fact a compromise between two requirements. On the one hand, the OMS is required to capture all actual system events. A high threshold can result in missing some of these events. On the other hand, the OMS is required to send warnings or control signals only when actual system events occur. A low threshold will trigger too many unnecessary calculations, even false alarms. Our solution is to use a relative conservative threshold, i.e. a relatively low threshold value. Any channel that has an event flag is further processed by prony or FDD analysis, and the results are

combined with moving window analysis and result crosschecks before warning signals are sent to the operators.

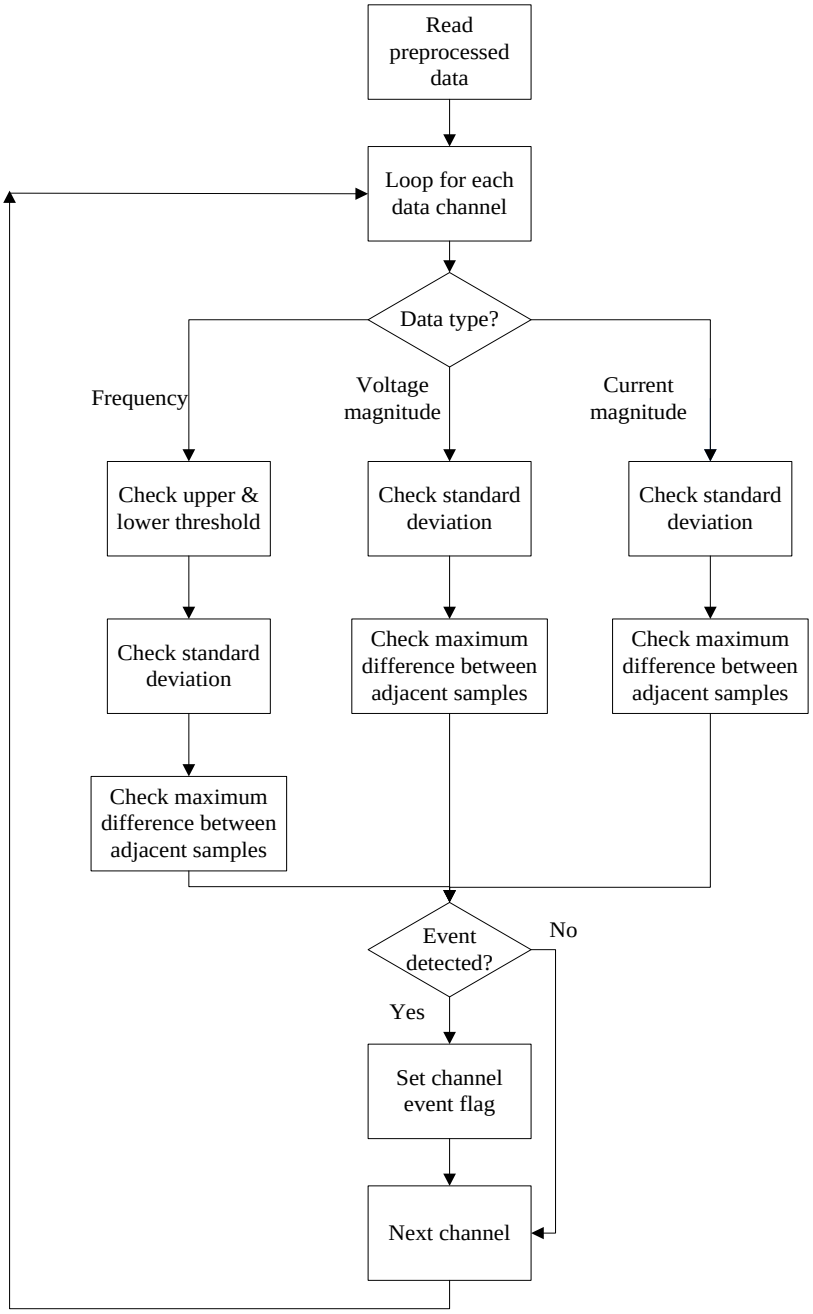

Fig. 2.2. Flowchart for event detection in the Oscillation Monitoring System

2.3.3. Moving Window Analysis and Result Crosschecks

The reason to conduct moving window analysis and crosschecks is to avoid

false alarms from the OMS. When a large disturbance occurs, the power system responses contain both linear and nonlinear phenomena following the disturbance. Moreover, presence of noise in the measurements can upset the accuracy of results. Typically, there are also many discrete switching events that occur during a routine disturbance event, and the damping of the modes can change after each of these switching events. Therefore, it is not uncommon to get different results from different methods, different signal groups or different time windows for the actual signals measured from power systems. Crosscheck is a crucial step to ensure the consistency of the online modal analysis.

In the proposed Oscillation Monitoring System, rules have been developed to crosscheck results from a) moving time-window analysis, b) multiple signal groups that contain modal responses, and c) different types of signal processing engines. Only when all the results are considered to be consistent will the system trigger an alarming signal, and here 'consistent' means the identified dominant modes from all the results fall into a pre-specified frequency range and damping ratio range. The choice of parameters in crosschecking is a trade-off between the speed of detection and accuracy.

2.3.3.1) Result crosscheck for post-disturbance measurements

The proposed Oscillation Monitoring System provides two levels of oscillation detection from post-disturbance measurements. That is, the OMS is able to detect local modes as well as inter-area modes. For the local oscillation detection, we use the signals from the same PMU. The signal groups used for local analysis are pre-specified. However, the pre-specified signal groups for inter-area mode may be not enough to capture some unexpected inter-area oscillations. For this reason, we also form the inter-area mode signal groups automatically from the subset of the PMUs that participate in the oscillations. All these tasks of local oscillation detection are executed in parallel by multi-threading in a powerful computer exclusively for oscillation monitoring in the control center.

After the local mode analysis, the next step is to determine the dominant mode in each PMU for each method, and then the crosscheck for all methods is performed in each PMU. The results are considered to be consistent if the dominant modes from different methods fall in a specified frequency range and damping ratio range. The above crosscheck is called local mode crosscheck. If more than two PMUs have consistent local crosschecks, then the inter-area mode detection tasks are activated. Inter-area mode crosscheck is performed from the subset of PMUs showing oscillations of the same frequency. Moving window crosscheck is to compare results along the sliding data windows. If several moving window crosschecks give consistent estimates, for example, four consecutive consistent moving windows crosschecks, then the resulting damping ratios are compared to a threshold to determine whether further action is needed. For instance, the damping ratio threshold for detecting poorly damped oscillations could be set to be say +3% for reliable operation of power systems. More detail and examples of PMU grouping for disturbance data processing can be found in Chapter 3.

2.3.3.2) Results crosscheck for ambient measurements

In the ambient data part of the OMS, the algorithm of FDD itself is able to handle multiple measurements. However, with the growing number of measurements, the computational burden for evaluating Power Density Spectrum matrix and the later SVD performed at each spectrum line, grows dramatically. Therefore, the capability of on-line computation requires only a small number of measurements used for each FDD analysis. With the fast spread of PMU installation across the power systems, we are now facing hundreds of PMU measurements at the control center. Then, it is important to group these measurements effectively to provide both local information and global view.

Our solution is a hierarchical structure similar as the one used in system disturbance part. In the lower level, we group the signals from each PMU and analyze many signal groups in a parallel manner by multi-threading of the FDD program.

Each PMU contains 5-10 signals, which is an ideal size for FDD. These individual PMUs contain local information, but they may produce inconsistent results for a global event. For this reason, we also form signal groups for global information in a higher level. The signal groups are formed automatically when more than one local PMU indicate insufficient damping at a similar frequency. The signals are drawn from these PMUs which show similar dominant frequency component, and analyze them by FDD. This gives a more consistent view for events involving many PMUs.

CHAPTER THREE

OSCILLATION MONITORING USING SYSTEM DISTURBANCE DATA

In this chapter, we summarize our efforts to develop an automatic oscillation monitoring system which is a rule-based expert system that monitors post-disturbance PMU measurements in real-time to detect the danger of growing or poorly damped oscillations in the early stages of the event. Three modal analysis methods from signal processing theory are used in this chapter, namely, Prony's Method, Matrix Pencil Method and Hankel Total Least Square (HTLS) method. All these methods try to fit a sum of exponential terms to the uniformly sampled data.

The prony analysis of real-time system disturbance data or event recordings in power systems is especially challenging because the power system responses contain both linear and nonlinear phenomena. Moreover, presence of noise in the measurements can upset the accuracy of results. Typically, there are also many discrete switching events that occur during a routine disturbance event, and these damping of the modes can change after each of these switching events. In the oscillation monitoring system developed at WSU, three types of rules have been developed to crosscheck results from a) moving time-window analysis, b) multiple signal groups that contain modal responses, and c) different types of signal processing engines, in order to ensure consistency of the modal analysis.

This chapter is organized as follows. Section 3.1 provides the common mathematical model for all the following algorithms. In section 3.2, Prony's method, Matrix Pencil Method and Hankel Total Least Squares (HTLS) are introduced and compared. The application of modal analysis engine following large disturbances is discussed in Section 3.3, followed by actual testing cases from real power system measurements in Section 3.4.

3.1. Linear Analysis of Power System Small Signal Stability

The power system is a high-order nonlinear system. However, for analyzing small disturbances, we can linearize a system around its operation point (or the equilibrium point). The linearized system can be simplified into the following form:

$$\begin{aligned} \Delta\dot{x} &= A\Delta x + b\Delta u \\ \Delta y_i &= c_i \Delta x \end{aligned} \quad , \quad i = 1,2,...,m \tag{3.1}$$

where Δx are the state vector, *b* and *c* are the input and output vectors respectively, Δu is the input and Δy_i is the output. As shown in [3], the transfer functions between the input and output has the following form,

$$G_i(s) = \frac{\Delta y_i(s)}{\Delta u(s)} = \sum_{i=1}^{n} \frac{R_i}{s - \lambda_i} \tag{3.2}$$

where $R_i = c_i \phi_i \psi_i b$, ϕ_i and ψ_i are right eigenvector and left eigenvector corresponding to λ_i respectively.

If we apply an impulse as input to the system, the *m* outputs are

$$y_j(t) = \sum_{i=1}^{n} R_i \exp(\lambda_i t), \quad j = 1,2,...m \tag{3.3}$$

If the input is not an impulse, e.g. a step input, the linearized system response will still be a sum of exponential terms. This is the form that our methods can be applied to for modal estimation. When $y_j(t)$ is sampled at a constant sampling period Δt, we get the following discrete form.

$$y(k) = \sum_{i=1}^{n} R_i z_i^k \tag{3.4}$$

where $z_i = \exp(\lambda_i \Delta t)$, $\lambda_i = \sigma_i + j\varpi_i$. *n* is called the model order, which is not known for real power system measurements.

3.2. Engines for Modal Analysis

We summarize the three signal processing engines in this section mainly aimed

at providing an introduction. Each method has its own advantages and weaknesses.

3.2.1. Prony's Method

Prony's Method tries to fit a sum of exponential terms to the uniformly sampled data. It was originally developed by *Baron de Prony* in 1795 to explain the expansion of various gases [35]. Prony analysis and classical eigenanalysis have become two standard approaches to study the problem of power system small signal stability [36]-[38]. The main steps are summarized below.

First, (3.4) can be written in the following form.

$$\begin{bmatrix} y(0) \\ y(1) \\ \\ y(N-1) \end{bmatrix} = \begin{bmatrix} 1 & 1 & ... & 1 \\ z_1 & z_2 & ... & z_n \\ ... & ... & ... & ... \\ z_1^{N-1} & z_2^{N-1} & ... & z_n^{N-1} \end{bmatrix} \begin{bmatrix} R_1 \\ R_2 \\ ... \\ R_n \end{bmatrix} \tag{3.5}$$

The z_i's are necessarily the roots of a *n*th-order polynomial with unknown coefficients a_i, and thus satisfy

$$z^n - (a_1 z^{n-1} + a_2 z^{n-2} + ... + a_n z^0) = 0 \tag{3.6}$$

If we left-multiply $[-a_n,-a_{n-1},...,-a_1,1,0,...0]$ to the both sides of (3.5), then we get the following equation using (3.6).

$$[-a_n,-a_{n-1},...,-a_1,1,0,...0] \begin{bmatrix} y(0) \\ y(1) \\ \\ y(N-1) \end{bmatrix} = 0 \tag{3.7}$$

We can left-multiply $[0,-a_n,-a_{n-1},...,-a_1,1,0,...0]$ to the both sides of (3.5) and the resulting right hand side is also zero.

Next, (3.7) can be repeated to get the following form.

$$\begin{bmatrix} y(n) \\ y(n+1) \\ \\ y(N-1) \end{bmatrix} = \begin{bmatrix} y(n-1) & y(n-2) & ... & y(0) \\ y(n) & y(n-1) & ... & y(1) \\ ... & ... & ... & ... \\ y(N-2) & y(N-3) & ... & y(N-n-1) \end{bmatrix} \begin{bmatrix} a_1 \\ a_2 \\ ... \\ a_n \end{bmatrix} \tag{3.8}$$

We can summarize the procedure of Prony's Method in the following three steps.

Step 1. Solve (3.8) to get the coefficients a_i.

Step 2. Calculate the roots of (3.6) to get z_i.

Step 3. Solve (3.5) for complex residues R_i.

Prony's Method can be extended to analyze multiple signals simultaneously. In step 1, we stack equations for each signal in (3.8). Consider a set of m signals $y_j(t)$, $j = 1,2,...m$. Now we have a total of $(N-n)\times m$ equations with n unknown coefficients a_i in (3.8). The coefficients a_i are solved in the least-square sense. After calculating roots z_i, Step 3 becomes solving the following equations.

$$\begin{bmatrix} y_1(0) & y_2(0) & ... & y_m(0) \\ y_1(1) & y_2(1) & ... & y_m(1) \\ ... & ... & ... & ... \\ y_1(N-1) & y_2(N-1) & ... & y_m(N-1) \end{bmatrix} = \begin{bmatrix} 1 & 1 & ... & 1 \\ z_1 & z_2 & ... & z_n \\ ... & ... & ... & ... \\ z_1^{N-1} & z_2^{N-1} & ... & z_n^{N-1} \end{bmatrix} \begin{bmatrix} R_1^1 & R_1^2 & ... & R_1^m \\ R_2^1 & R_2^2 & ... & R_2^m \\ ... & ... & ... & ... \\ R_n^1 & R_n^2 & ... & R_n^m \end{bmatrix} \quad (3.9)$$

A practical issue in Prony's Method is to determine the unknown model order *n*. The common procedure is to fit a high order model to the data, and the modes corresponding to the noise have small residue magnitudes that can be filtered out from the result.

3.2.2. Matrix Pencil Method

The idea of Matrix Pencil method comes from the pencil-of-function approach. It is used in the areas like system identification and spectrum estimation [39]-[42]. The main steps of Matrix Pencil method are shown below.

First, define two matrices as follows.

$$[Y_1]=\begin{bmatrix} x(0) & x(1) & ... & x(L-1) \\ x(1) & x(2) & ... & x(L) \\ ... & ... & ... & ... \\ x(N-L-1) & x(N-L) & ... & x(N-2) \end{bmatrix} \tag{3.10}$$

$$[Y_2]=\begin{bmatrix} x(1) & x(2) & ... & x(L) \\ x(2) & x(3) & ... & x(L+1) \\ ... & ... & ... & ... \\ x(N-L) & x(N-L+1) & ... & x(N-1) \end{bmatrix} \tag{3.11}$$

where *x(k)* are the noise-free data points. *L* is the pencil parameter.

Using (3.4), we can write (3.10) and (3.11) as

$$[Y_2]=[Z_1][R][Z_0][Z_2] \tag{3.12}$$

$$[Y_1]=[Z_1][R][Z_2] \tag{3.13}$$

where

$$[Z_2]=\begin{bmatrix} 1 & z_1 & ... & z_1^{L-1} \\ 1 & z_2 & ... & z_2^{L-1} \\ ... & ... & ... & ... \\ 1 & z_n & ... & z_n^{L-1} \end{bmatrix}_{n\times L} \quad [Z_1]=\begin{bmatrix} 1 & 1 & ... & 1 \\ z_1 & z_2 & ... & z_n \\ ... & ... & ... & ... \\ z_1^{N-L-1} & z_2^{N-L-1} & ... & z_n^{N-L-1} \end{bmatrix}_{(N-L)\times n}$$

$$[Z_0]=diag[z_1, z_2, ...z_n]$$

$$[R]=diag[R_1, R_2, ...R_n]$$

where *diag[]* represents a diagonal matrix.

The matrix pencil is defined as follows.

$$[Y_2]-\lambda[Y_1]=[Z_1][R]\{[Z_0]-\lambda[I]\}[Z_2] \tag{3.14}$$

where [*I*] is identity matrix.

When $n \le L \le N-n$, the rank of $\{[Y_2]-\lambda[Y_1]\}$ is n if $\lambda \ne z_i$ [39]. However, if $\lambda = z_i$, then the *i*-th row of $\{[Z_0]-\lambda[I]\}$ becomes zero, and the rank of $\{[Y_2]-\lambda[Y_1]\}$ is reduced by one. Hence, the parameters z_i's are the generalized eigenvalues of the matrix pair $\{[Y_2];[Y_1]\}$. Or, equivalently, we can solve the

ordinary eigenvalues of $\{[Y_1]^+[Y_2]-\lambda[I]\}$ to get the parameters z_i, where $[Y_1]^+$ is pseudo-inverse of $[Y_1]$. After solving for parameters z_i, we solve (3.5) for residues.

For the actual measured data, define a new matrix $[Y]$ containing the noisy data as follows.

$$[Y]=\begin{bmatrix} y(0) & y(1) & ... & y(L) \\ y(1) & y(2) & ... & y(L+1) \\ ... & ... & ... & ... \\ y(N-L-1) & y(N-L) & ... & y(N-1) \end{bmatrix} \tag{3.15}$$

Comparing to (3.10) and (3.11), we can see that $[Y_1]$ is obtained by deleting the last column of $[Y]$, and $[Y_2]$ is obtained by deleting the first column of $[Y]$.

Next, apply SVD to $[Y]$ as follows.

$$[Y]=U\Sigma V^H \tag{3.16}$$

where U and V are unitary matrices. Σ is a diagonal matrix containing the singular values of $[Y]$ with descending order. The superscript H denotes conjugate transpose.

If the data were noise free, the matrix $[Y]$ has n nonzero singular values. However, when noise is present, the zero singular values are perturbed and become nonzero. Now, the Singular Value Decomposition provides an effective way of noise filtering. The singular values below some specified threshold are considered to be caused by noise and need to be set as zero.

Then, we use the n significant singular values to reconstruct the original data matrix. Now, we have

$$[V']=[v_1, v_2, ...v_n] \tag{3.17}$$

$$[Y_1]=U\Sigma'[V_1']^H \tag{3.18}$$

$$[Y_2]=U\Sigma'[V_2']^H \tag{3.19}$$

where $v_i's$ are column vectors of V corresponding to the n dominant singular

values. Σ' is the first n columns of Σ. $[V_1^{'}]$ is obtained from $[V']$ with the last column of $[V']$ deleted. $[V_2^{'}]$ is obtained from $[V']$ with the first column of $[V']$ deleted.

Now, we have

$$[Y_1]^{+}[Y_2] = [V_1^{'} * V_1^{'H}]^{-1} * V_1^{'} * V_2^{'H} = [V_1^{'H}]^{+} V_2^{'H}$$

The nonzero eigenvalues of $[V_1^{'H}]^{+} V_2^{'H}$ are the same as the eigenvalues of $V_2^{'H}[V_1^{'H}]^{+}$, where $V_2^{'H}[V_1^{'H}]^{+}$ is an $n \times n$ matrix. Calculating the eigenvalues of an $n \times n$ matrix is computationally inexpensive since n is usually a small number. After the eigenvalues are obtained, solve (3.5) for the residues.

3.2.3. Hankel Total Least Square (HTLS) Method

HTLS method is a more recent method and it also fits an exponential decay model onto a waveform. It is proposed in papers [43], [44], and the main steps are summarized next.

First, form the Hankel matrix as follows.

$$H = \begin{bmatrix} y_0 & y_1 & \cdots & y_{M-1} \\ y_1 & y_2 & \cdots & y_M \\ \cdots & \cdots & \cdots & \cdots \\ y_{L-1} & y_L & \cdots & y_N \end{bmatrix} \tag{3.20}$$

where L is a parameter chosen to be larger than n, $M = N + 1 - L$, N is the number of measurements.

If there is no noise, i.e $y(k) = \sum_{i=1}^{n} R_i z_i^k$, then H can be factorized as follows.

$$H = \begin{bmatrix} 1 & \cdots & 1 \\ z_1^1 & \cdots & z_n^1 \\ \cdots & \cdots & \cdots \\ z_1^L & \cdots & z_n^L \end{bmatrix} \begin{bmatrix} R_1 & & \\ & \ddots & \\ & & R_n \end{bmatrix} \begin{bmatrix} 1 & z_1^1 & \cdots & z_1^{M-1} \\ \cdots & \cdots & \cdots & \cdots \\ \cdots & \cdots & \cdots & \cdots \\ 1 & z_n^1 & \cdots & z_n^{M-1} \end{bmatrix}$$

$$= SRT^T \tag{3.21}$$

where both *S* and *T* are Vandermonde matrices.

The matrix *S* is shift-invariant, that is

$$S_{\downarrow} Z = S_{\uparrow} \tag{3.22}$$

where the up (down) arrow placed behind a matrix stands for deleting the top (bottom) row of the matrix and *Z* is the $n \times n$ diagonal matrix whose diagonal entries are $z_1, ..., z_n$.

The Hankel matrix can also be decomposed by SVD as follows.

$$H = U \Sigma V^H = \begin{bmatrix} \hat{U} & U_0 \end{bmatrix} \begin{bmatrix} \hat{\Sigma} & \\ & \Sigma_0 \end{bmatrix} \begin{bmatrix} \hat{V} \\ V_0 \end{bmatrix}^H \tag{3.23}$$

where *U* and *V* and unitary matrix, i.e $UU^H = I$, $VV^H = I$, *I* is identity matrix, *H* denotes complex conjugate transpose. Σ is a diagonal matrix with singular values on the diagonal in decreasing order. $\hat{\Sigma}$ is the submatrix containing first *n* singular values. If there is no noise in the signal, the submatrix Σ_0 is null. Otherwise, Σ_0 is a full matrix with small singular values on the diagonal. When noise is present, the usual procedure is to set a threshold and those singular values below the threshold are considered to be generated by noise and can be discarded.

In the noise-free case, $H = \hat{U} \hat{\Sigma} \hat{V}^H$. Compare this equation with (3.21), we have the following relationship.

$$\hat{U} = SQ \tag{3.24}$$

where *Q* is a *n* by *n* nonsingular matrix. Deleting the last row in the above equation gives $\hat{U}_{\downarrow} = S_{\downarrow} Q$, while deleting the first row gives $\hat{U}_{\uparrow} = S_{\uparrow} Q$.

Thus $\hat{U}_{\downarrow}$ and $\hat{U}_{\uparrow}$ are related by the following equation.

$$\hat{U}_{\uparrow} = S_{\downarrow} ZQ = \hat{U}_{\downarrow} Q^{-1} ZQ = \hat{U}_{\downarrow} \tilde{Z} \tag{3.25}$$

where $\tilde{Z} = Q^{-1} ZQ$, which has the same eigenvalues as *Z*, ie. $z_1, ..., z_n$.

In the noisy case, equation (3.25) does not hold exactly. In this case, we solve $\tilde{Z}$ by total lease square method. After calculating $\tilde{Z}$, the signal poles are calculated as the eigenvalues of $\tilde{Z}$.

When we need to analyze multiple signals simultaneously, simply replace *H* in (3.20) by the horizontally stacked Hankel matrices as follows.

$$H_{series} = \begin{bmatrix} H_1 & H_2 & \dots & H_m \end{bmatrix} \tag{3.26}$$

where *m* is the number of signals.

The last step to calculate residues R_i's is the same as that of Prony's method.

3.2.4. Comparison of Three Methods

Given three analysis methods described above, we are now interested in comparing their performances. The accuracy of the estimated frequency and damping ratio under noisy measurement is of special interest to our problem. In the following, we add different levels of noise to the data, and then calculate the mean value and standard deviation of the estimated frequencies and damping ratios from 100 independent runs. The test signal used for comparison is shown below.

$$y(t) = e^{-0.05t}\cos(2\pi * 0.2t) + e^{-0.1t}\cos(2\pi * 0.3t) + n(t)$$

where *n(t)* denotes noise component. *y(t)* is sampled at 30 Hz and a total of 10 seconds data is used for analysis.

The signal contains two modes at 0.2 and 0.3 Hz with damping ratio of 3.98% and 5.30% respectively. A hundred simulation runs for each Signal-Noise-Ratio (SNR) level and each method are carried out and the results are shown in Table 3.1 and 3.2. For Matrix Pencil method and HTLS method, the SVD threshold is set to 10% of the largest singular value.

From Tables 3.1 and 3.2, we can see that all of the three methods can estimate the frequencies of both modes quite accurately. However, damping ratio estimation, which is more important in oscillation monitoring, has larger variance, especially

under higher noise level. For example, at the 20 dB SNR level, the standard deviations of the estimated damping ratio of the first mode are 1.41%, 0.99% and 0.92% for Prony's Method, Matrix Pencil and HTLS respectively. These standard deviations are comparable to the mean values, and this indicates we get less reliable estimation results when the noise is high. Among the three methods, Matrix Pencil Method and HTLS method have similar noise performance, and they are better than Prony's Method as shown by their standard deviations. In other words, Prony's Method is more sensitive to noise.

TABLE 3.1
COMPARISON OF THREE METHODS UNDER NOISY MEASUREMENTS
(30 DB NOISE)

	Frequency (Hz)	Damping Ratio (%)	Frequency (Hz)	Damping Ratio (%)
True Value	0.2000	3.98	0.3000	5.30
Mean Value (Prony's Method)	0.1999	4.12	0.2999	5.20
Standard Deviation (Prony's Method)	0.0008	0.74	0.0013	0.38
Mean Value (Matrix Pencil)	0.1990	4.05	0.3031	4.93
Standard Deviation (Matrix Pencil)	0.0004	0.26	0.0005	0.16
Mean Value (HTLS)	0.1990	4.07	0.3032	4.89
Standard Deviation (HTLS)	0.0004	0.26	0.0005	0.18

TABLE 3.2
COMPARISON OF THREE METHODS UNDER NOISY MEASUREMENTS
(20 DB NOISE)

	Frequency (Hz)	Damping Ratio (%)	Frequency (Hz)	Damping Ratio (%)
True Value	0.2000	3.98	0.3000	5.30
Mean Value (Prony's Method)	0.1991	3.97	0.3010	4.84
Standard Deviation (Prony's Method)	0.0017	1.41	0.0021	1.15
Mean Value (Matrix Pencil)	0.1990	4.11	0.3031	4.91
Standard Deviation (Matrix Pencil)	0.0012	0.99	0.0017	0.68
Mean Value (HTLS)	0.1988	3.86	0.3036	5.01
Standard Deviation (HTLS)	0.0011	0.92	0.0015	0.65

Next, a comparison of the speeds of three methods is performed and the average time needed for one simulation run is shown in Table 3.3. For Prony's method, the speed depends on how we solve the least squares problem (section 3.2.1). The SVD based least square procedure is numerically more robust than the QR based procedure, but it is much more time-consuming since SVD is an $O(n^3)$ procedure. For Matrix Pencil and HTLS method, they have similar procedure of SVD for the Hankel matrix. The result in Table 3.3 shows that the HTLS method is relatively the fastest among the three methods.

The average computational times reported in Table 3.3 were computed using Matlab code running in a "typical" three-year old laptop. The times are meant for relative comparison among the three methods. In actual field implementation with efficient C code, the algorithms are quite fast as reported in [29].

TABLE 3.3
AVERAGE TIME NEEDED FOR ONE SIMULATION RUN

Methods	Average Time (sec)
Prony (SVD)	0.44983
Prony (QR)	0.12250
Matrix Pencil	0.17046
HTLS	0.11625

3.3. Oscillation Monitoring Following Large Disturbances

Power system is basically a high-order nonlinear system. These nonlinearities are caused by many factors such as the fundamentally nonlinear nature of power balance equations, the limiting functions in exciters, Power System Stabilizers (PSS), etc., the nonlinearities of generator saturation curves as well as nonlinear load responses in the system [45]. The power system responses following large disturbances usually show strong nonlinearities, especially immediately following a line outage when the field currents in the exciters may hit the upper limits trying to

boost generator terminal voltages. If the system is transient stable, the system should move to the previous or a new operating point in the form of a damped oscillatory response which is also sometimes referred to as the “ring-down”.

In [7], the authors apply the Hilbert spectral analysis to the responses following the fault and obtain the instantaneous frequency and damping. The resulting instantaneous damping ratios are comparable to the damping ratio from prony analysis. However, the instantaneous damping varies much after fault, and it has to be averaged over time to provide useful information.

In the following paragraph, we will show that the proposed OMS is able to give good estimate for the ring-down case following a large disturbance. The test system is a two-area four-generator system from [3]. The one-line diagram of the system is shown as follows.

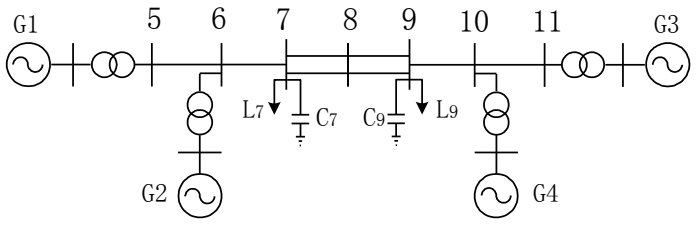

Fig. 3.1. One line diagram of two-area system

The operating condition and system parameters are the same as those in [3]. Note that only two PSS’s are installed on G1 and G3 respectively. The complete eigenvalue analysis is done using SSAT [46] for the system. The original system has an inter-area mode with 0.6176 Hz and 5.35% damping ratio. When line 7-8 circuit #1 is out of service, the inter-area mode will change to 0.4589 Hz and 4.70% damping ratio. Now, for the original system, we apply a three-phase fault using TSAT [47] in the middle of the line 7-8 circuit #1, and clear the fault after 0.1 sec. by tripping the faulted line. No reclosing action is performed and the active power of the parallel line 7-8 circuit #2 is shown below.

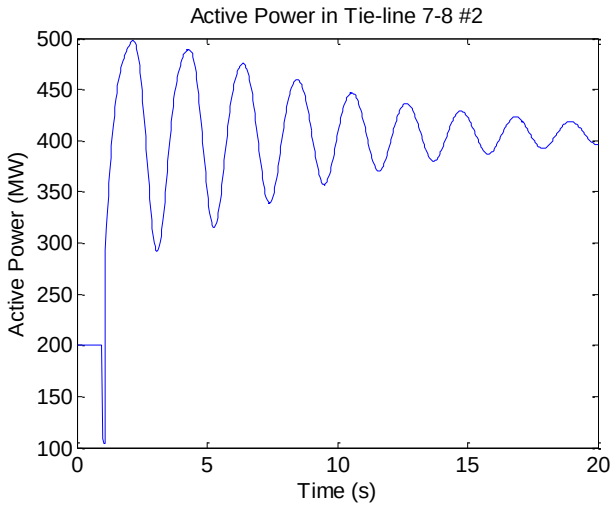

Fig. 3.2. Active powers of line 7-8 circuit #2 following a 0.1 sec three phase line fault

The three methods are applied to the above tie-line active powers using a 5 second sliding window after the fault and the resulting frequency and damping ratio are plotted at the end of each analysis window in Fig. 3.3. The upper part of the plot shows the frequency estimates and the lower part shows the damping ratio estimates.

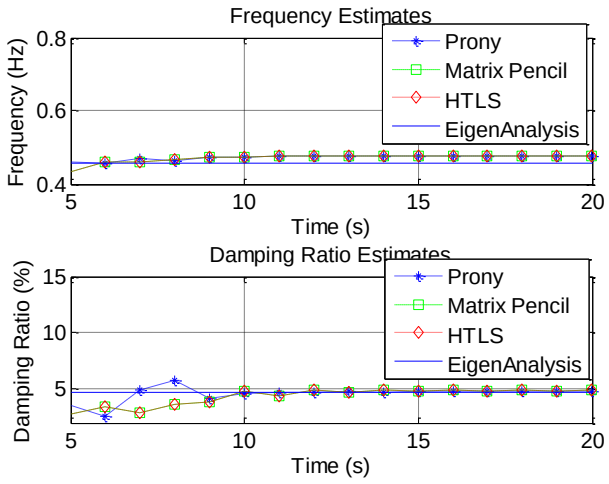

Fig. 3.3. Frequency and damping ratio estimates following a 0.1 sec three phase line fault

From Fig. 3.3, we clearly see the nonlinear effects on the analysis results. In the first few swings after the fault, the damping ratios from three methods are different from each other and they also differ a lot from the result from eigenanalysis. The nonlinearities in the first few swings from factors such as saturations and exciter limiters can result in an underestimate (or overestimate) of damping ratio for the inter-area mode. From linear system theory, we note that the concepts of eignevalues and modal analysis are only applicable for small disturbances away from an equilibrium point. It is imperative that we ignore the results of modal analysis when the system responses are large in being away from the equilibrium point. However, after the first few swings, the three methods give consistent and accurate damping ratio estimates. This test shows the importance of avoiding the adverse effect of nonlinearities. In the proposed OMS, the first one or two swings are ignored immediately after the fault by our consistency crosscheck rules in order not to trigger false warning signals.

3.4. Case Studies for Oscillation Monitoring

3.4.1. Case I

In this test case, we will apply three methods to PMU measurements recorded in WSCC system on August 4th, 2000. At about 19:56 GMT Standard Time, the Alberta system separated from the rest of the system, resulting in poorly damped oscillations [48]. The voltage magnitude at Malin Substation is shown in Fig. 3.4. The 0.27 Hz inter-area mode involved in this event appears to be the same inter-area mode that led to the August 10th, 1996 WSCC blackout. The solid black vertical line in the middle of the figure shows the time instant when the OMS issues an alarm. This is explained in more detail in the following paragraphs.

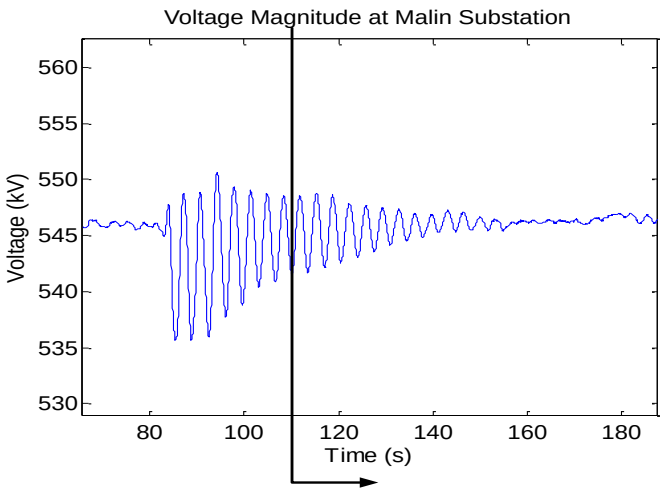

Fig. 3.4. The voltage magnitude at Malin in Aug. 4, 2000

The recorded data contains measurements from a total of ten PMUs, eight of which are located at 500kV substations, including Grand Coulee, Malin, Colstrip, Devers etc. In the following analysis, we only use the measurements from these eight PMUs. First, we form signal groups in each PMU and cross-check their results for all methods. The signals used for analysis are voltage and current magnitudes in each PMU, while the frequency measurements are avoided because of lesser accuracy. A series of analyses using a 5-second sliding window are applied to the data segment from 60 sec. to 130 sec., where the time at 0 sec corresponds to 19:55:00 GMT Standard Time. The results are plotted at the end point of the sliding widow for each analysis. The frequency and damping ratio estimates shown in Fig. 3.5, 3.6 and 3.7 correspond to the results at Grand Coulee, Malin and Devers substation respectively. Again, the upper part of the plot shows the frequency estimates and the lower part shows the damping ratio estimates.

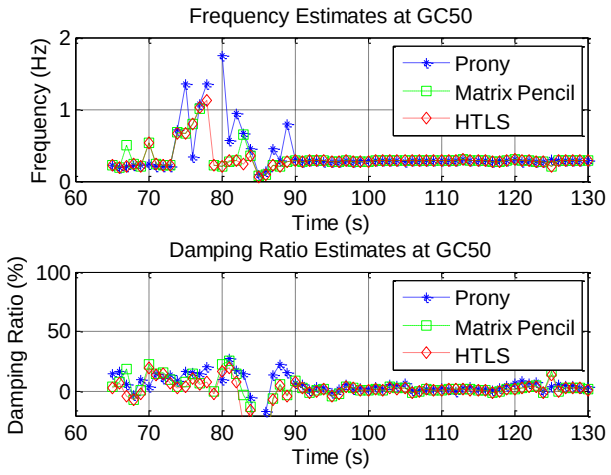

Fig. 3.5. Frequency and damping ratio estimates at Grand Coulee for Case I

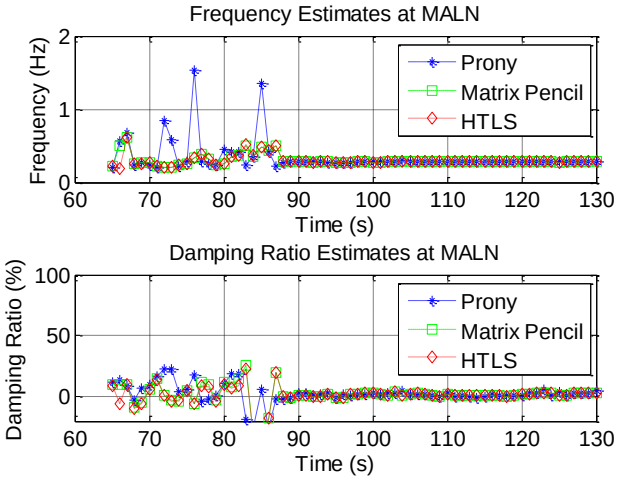

Fig. 3.6. Frequency and damping ratio estimates at Malin Substation for case I

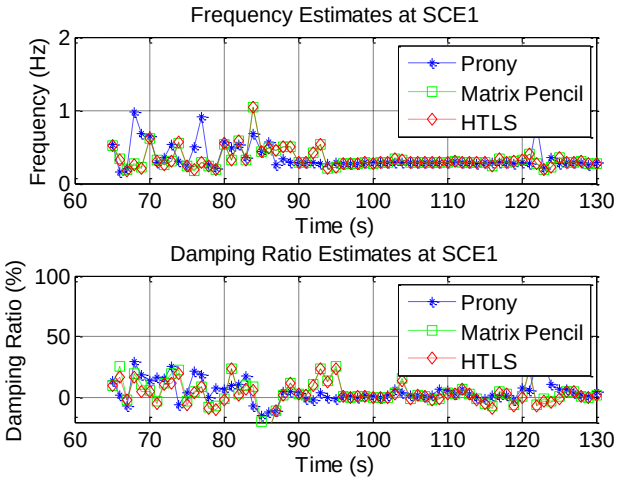

Fig. 3.7. Frequency and damping ratio estimates at Devers (SCE1) for case I

From the figures above, we see that the estimates become consistent for all three methods when the analysis window begins to cover the oscillation segment. Fig. 3.8 shows consistent estimates in all the PMUs, where each dot stands for a consistent estimate in the corresponding PMU. It is seen that the measurements at John Day, Malin and Keeler substations have more consistent estimates than others during this event. This is because these PMUs are located along main transmission corridors for the inter-area oscillation.

All three methods, Prony's Method, Matrix Pencil, and HTLS can compute for the mode shape associated with an inter-area mode when we use consistent measurements from each PMU in the inter-area mode detection stage above. That is, if we use all bus voltage measurements or bus voltage phase angles from different PMUs, the related residues and phase angles in the inter-area detection shape can give us valuable insight into the mode shape of that oscillatory mode.

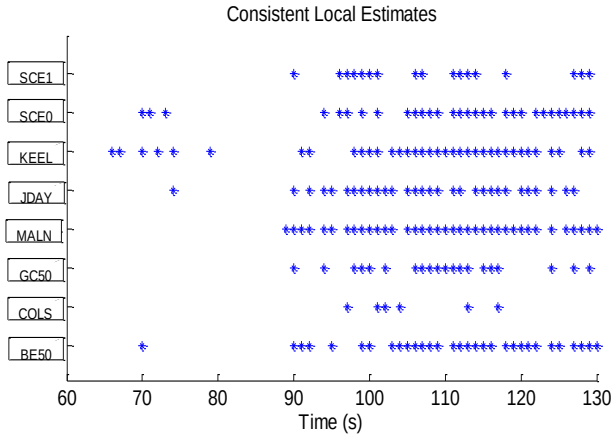

Fig. 3.8. Consistent local estimates in all PMUs for case I

When more than two consistent local crosschecks are found at a specific time, the inter-area mode detection is activated automatically. The signals used here for inter-area mode detection are voltage magnitudes at the PMUs showing consistent local crosschecks. The results for inter-area mode detection are shown in Fig. 3.9. An

acceptable result of a predefined number (say 4) of consecutive moving window consistent inter-area crosschecks occur at 109 sec., with the mean frequency at 0.2871 Hz and the mean damping ratio is +0.96%. Therefore, the OMS is able to trigger an alert to system operator with a reliable estimation at the early stage of the oscillation, showing a good compromise between the speed of detection and accuracy.

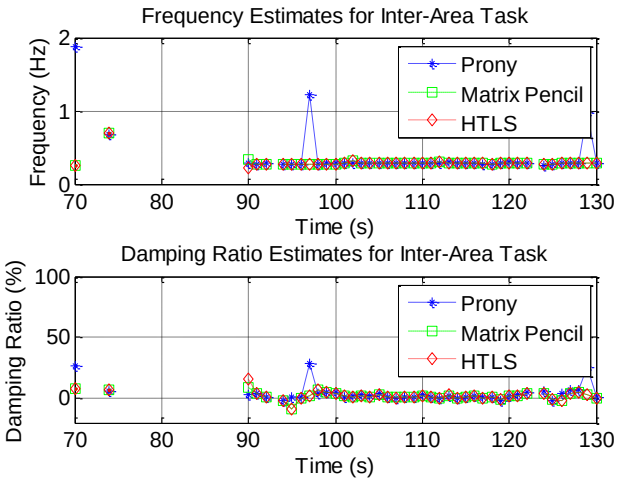

Fig. 3.9. Frequency and damping ratio estimates of inter-area oscillation detection for case I

3.4.2. Case II

The second case is recorded recently in eight PMUs located in TVA system [29]. After a 500kV line tripping, we can see an oscillation in the system. The voltage magnitude at one 500kV substation PMU 3 is plotted below for the initial stage of the oscillation. The bold black vertical line again shows the time instant when the OMS issues an alarm.

The measurements from each PMU form a signal group. A series of analyses using 5-second sliding window are applied to the data segment from 330 sec. to 360 sec. The consistent estimates for all PMUs are shown in Fig. 3.11. The results show that this event is either a local oscillation or an intra-area oscillation, and the problematic area is somewhere between PMU 2 and PMU 3. This information is also quite useful to choose appropriate damping controls.

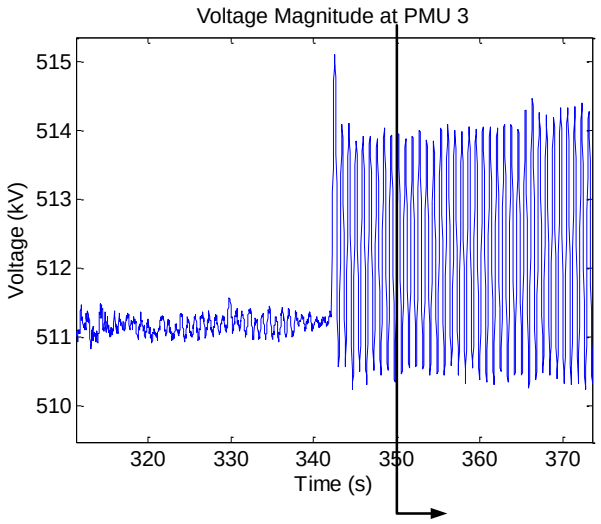

Fig. 3.10. The voltage magnitude at PMU 3 for case II

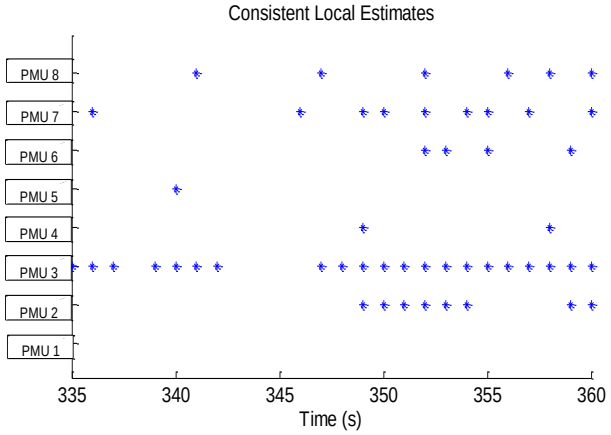

Fig. 3.11. Consistent local estimates in all PMUs for case II

The local crosscheck at PMU 3 is shown in Fig. 3.12. The inter-area crosscheck is activated automatically and the results are shown in Fig. 3.13. The OMS will trigger an alert at 350s, when the number of moving window consistent inter-area estimates reaches a predefined number say 4. The mean frequency is 1.1754 Hz and the mean damping ratio is +0.39% for the inter-area crosscheck. The local crosscheck at PMU 3 also gives a consistent estimate at 350s with the mean frequency at 1.1777 Hz and the damping ratio at 0.14%, The OMS will therefore issue an alarm or a control trigger thus indicating the need for some operator intervention or control action.

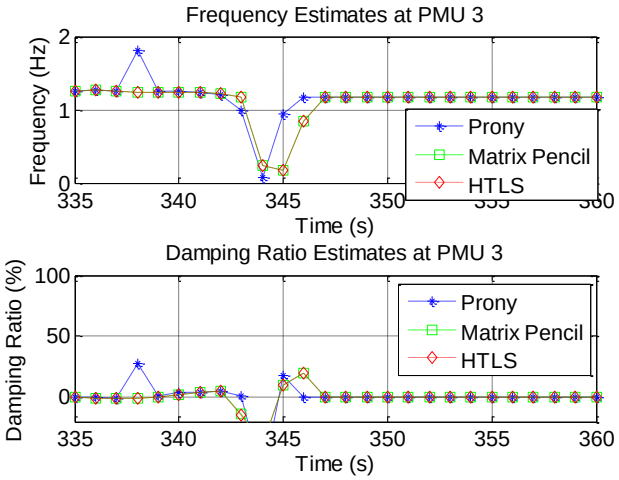

Fig. 3.12. Frequency and damping ratio estimates at PMU 3 for Case II

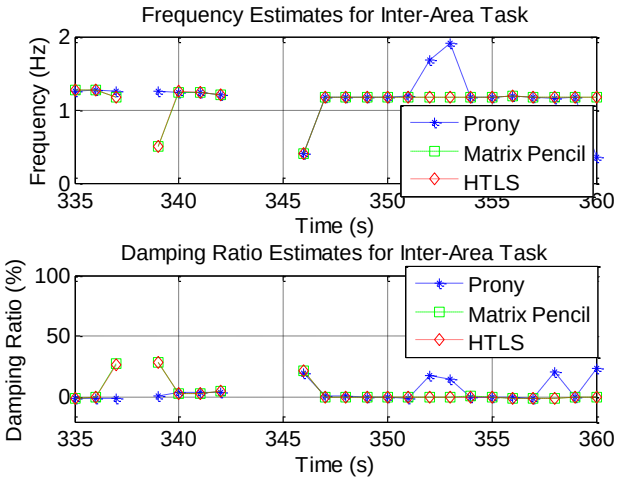

Fig. 3.13. Frequency and damping ratio estimates of inter-area oscillation detection for Case II

3.4.3. Case III

This case is also from the eastern interconnection in the US. Here we only have measurements from three PMUs, so the OMS will trigger an alarm when local moving window crosscheck reaches a consistent estimate. Again, the signal groups are formed in each PMU. The voltage magnitude at PMU 1 is shown in Fig. 3.14. The bold black vertical line shows the time instant when the Oscillation Monitoring System issues an alarm.

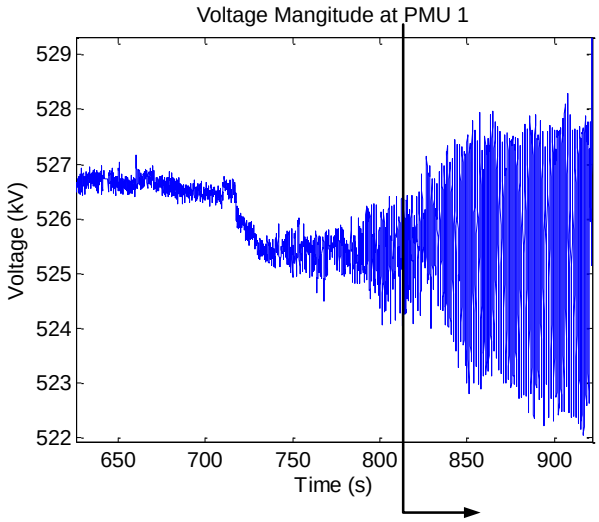

Fig. 3.14. The voltage magnitude at PMU 1 for case III

Sliding 5 second time-windows are applied to the data segment form 740 sec. to 820 sec. The results for the signal group from PMU 1 are shown in Fig. 3.15. Consecutive 4 moving window consistency crosschecks occur at 811 sec., with the mean frequency at 0.6892 Hz and the mean damping ratio of -0.59%. This shows that system operator may have seen an alert at the beginning stage of the oscillation if the OMS had been installed. The signal groups in other PMUs do not have consistent estimates, so they are not shown here. Had any damping control been applied in the early stage, the system may have avoided the eight minutes of sustained oscillation.

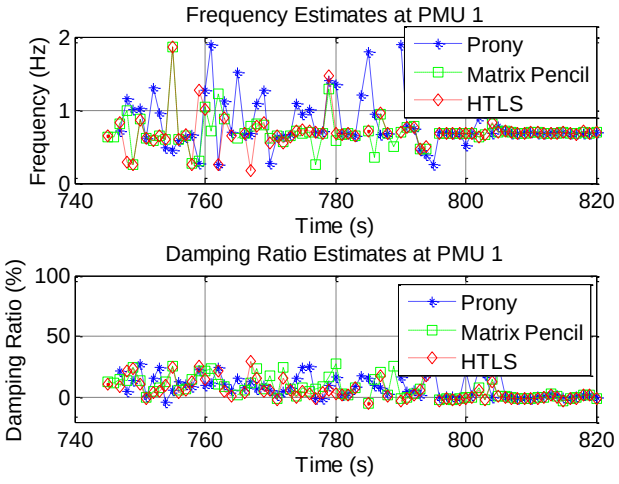

Fig. 3.15. Frequency and damping ratio estimates of PMU 1 for Case III

CHAPTER FOUR

OSCILLATION MONITORING USING AMBIENT DATA

In this chapter, we combine prony analysis with the original method of Frequency Domain Decomposition (FDD) towards real-time analysis of ambient measurements from PMUs in power systems for the purpose of oscillation monitoring. Unlike previous methods used for ambient data processing, this modified FDD is able to simultaneously identify damping and mode shape of the dominant mode using several minutes of ambient data.

The main idea of this approach is to apply Singular Value Decomposition (SVD) to the power density spectrum matrix. The resulting singular values and singular vectors can be further processed by prony analysis to obtain mode damping and mode shapes. Whenever one of the oscillatory modes moves toward the imaginary axis, i.e. damping of the mode decreases toward zero, the standard deviation of damping estimates decrease significantly, making it possible to capture the problematic mode before it becomes critical. The ambient data processing by FDD, together with the real-time post-disturbance monitoring in [6], constitute a complete Oscillation Monitoring System (OMS). A prototype version of this OMS has been implemented at Tennessee Valley Authority (TVA) [29].

This chapter is organized as follows. Section 4.1 presents the theoretical background and some implementation issues for Frequency Domain Decomposition. In Section 4.2, FDD is applied to simple linear systems to illustrate some of its important properties. In Section 4.3, FDD is applied to simulated response of a small power system. Section 4.4 discusses several case studies using real PMU measurements in power systems.

4.1. Frequency Domain Decomposition

4.1.1. Theoretical Background

4.1.1.1) Power Spectrum Representation

The high-order nonlinear power system model can be linearized around its equilibrium point and expressed in the state space form as follows [3, Page 703],

$$\begin{aligned} \Delta\dot{x} &= A\Delta x + B\Delta u \\ \Delta y &= C\Delta x + D\Delta u \end{aligned} \tag{4.1}$$

where Δx, Δu, Δy are the state, input and output vector respectively.

Assume that Δy is not a direct function of Δu (i.e. D = 0), then the transfer function matrix between the inputs and outputs has the following form [3, Page 720],

$$H(s) = \sum_{i=1}^{n} \frac{R_i}{s - \lambda_i} \tag{4.2}$$

where $\lambda_i = -\alpha_i + j\omega_i$ is the eigenvalue of A. $R_i = C\phi_i\psi_i B$, where ϕ_i and ψ_i are the right and left eigenvector corresponding to λ_i respectively. And n is the order of the system model. Note that s and λ_i are scalars and R_i is a matrix.

For a stationary random process $y(t)$, its autocorrelation function is defined as $\gamma_{yy}(\tau) = E[y^*(t)y(t+\tau)]$, where the symbol * and E stand for complex conjugate and expectation respectively. The *power density spectrum* or *power spectral density (PSD)* $S(\omega)$ is the Fourier transform of the above autocorrelation function by Wiener-Khintchine theorem [49, Page 902]. For a single-input single-output (SISO) system, the input and output power density spectrum has a simple relationship as $S_{yy}(\omega) = |H(\omega)|^2 S_{uu}(\omega)$. In the multi-input multi-output (MIMO) case, the relationship is extended as follows [50, Page 263].

$$S_{yy}(\omega) = H(j\omega) \cdot S_{uu}(\omega) \cdot H(j\omega)^H \tag{4.3}$$

where the superscript H denotes complex conjugate transpose.

If the inputs are white noise, the power spectrum $S_{uu}(\omega)$ will be a constant diagonal matrix, denoted by *F*. In Appendix A, the following expression of $S_{yy}(\omega)$ for white noise inputs is derived,

$$S_{yy}(\omega) = \sum_{i=1}^{n} \left[\frac{A_i}{j\omega - \lambda_i} - \frac{A_i^H}{j\omega + \lambda_i^*} \right] \tag{4.4}$$

where $A_i = R_i F \sum_{k=1}^{n} \frac{-R_k^H}{\lambda_i + \lambda_k^*}$.

4.1.1.2) Power Spectrum Decomposition and SVD

The peaks in $S_{yy}(\omega)$ can correspond to poorly damped modes of the system when such modes exist in the system. In the following subsections, we will show that the inverse FFT of decomposed spectrum $S_{yy}(\omega)$ has an exponential form and can be further processed by prony analysis. This is different from the post-disturbance type methods which apply prony analysis to the measured data directly. First, we will start the theoretical derivation from the following two observations when $S_{yy}(\omega)$ is evaluated near the frequency of a poorly damped mode $\lambda_r = -\alpha_r + j\omega_r$.

4.1.1.2.1) $S_{yy}(\omega)$ evaluated near ω_r can be approximated by a rank one matrix, if there is no significant contribution from other poorly damped modes nearby.

The *r*-th residue term A_r has the following form.

$$\begin{aligned} A_r &= R_r F \sum_{k=1}^{n} \frac{-R_k^H}{\lambda_r + \lambda_k^*} = \frac{-R_r F R_r^H}{\lambda_r + \lambda_r^*} + R_r F \sum_{\substack{k=1 \\ k \neq r}}^{n} \frac{-R_k^H}{\lambda_r + \lambda_k^*} \\ &= \frac{R_r F R_r^H}{2\alpha_r} + R_r F \sum_{\substack{k=1 \\ k \neq r}}^{n} \frac{-R_k^H}{\lambda_r + \lambda_k^*} \end{aligned} \tag{4.5}$$

When α_r is small, i.e. when λ_r is close to the imaginary axis in the complex s-plane, the first term is much larger than the remaining terms, so A_r can be

approximated as $\frac{R_r F R_r^H}{2\alpha_r}$ and now $A_r = A_r^H$. If there are no other poorly damped modes near ω_r, then the contributions from the other terms in (4.4) are negligible for $S_{yy}(\omega)$ near ω_r. $S_{yy}(\omega)$ can be approximated as follows,

$$S_{yy}(\omega)|_{\omega \text{ near } \omega_r} \approx \frac{A_r}{\alpha_r + j(\omega - \omega_r)} - \frac{A_r}{-\alpha_r + j(\omega - \omega_r)}$$

$$= \frac{R_r F R_r^H}{\alpha_r^2 + (\omega - \omega_r)^2} \tag{4.6}$$

Let $R_i = w_i l_i^H$, where $w_i = C\phi_i$ and $l_i^H = \psi_i B$. Note that w_i is the mode shape for mode *i* when *C* is an identity matrix. i.e it is possible to extract mode shape information when state variables are observed. Now,

$$S_{yy}(\omega)|_{\omega \text{ near } \omega_r} \approx \frac{w_r l_r^H F l_r w_r^H}{\alpha_r^2 + (\omega - \omega_r)^2}$$

$$= \frac{w_r d_r w_r^H}{\alpha_r^2 + (\omega - \omega_r)^2} = s_r(\omega) w_r w_r^H \tag{4.7}$$

where $d_r = l_r^H F l_r$ and $s_r(\omega) = \frac{d_r}{\alpha_r^2 + (\omega - \omega_r)^2}$ are scalars. And the expression in (4.7) is a rank one matrix.

4.1.1.2.2) The rank determined by SVD of $S_{yy}(\omega)$ corresponds to the number of contributing modes when $S_{yy}(\omega)$ is evaluated near ω_r.

If there are several poorly damped modes near ω_r, there will be more terms in (4.7). For example, if $\lambda_i = -\alpha_i + j\omega_i$ has small α_i and ω_i is close to ω_r, then $\alpha_i^2 + (\omega - \omega_i)^2$ is also small when evaluating $S_{yy}(\omega)$ near ω_r. Usually the number of these terms in (4.7) is small. If we sort these $s_i(\omega)$'s by their influence on $S_{yy}(\omega)$

near ω_r in decreasing order and take only the first n_o terms, then $S_{yy}(\omega)$ near ω_r can be expressed as

$$S_{yy}(\omega)|_{\omega near \omega_r} \approx \begin{bmatrix} w_{r,1},...,w_{r,n_o} \end{bmatrix} \begin{bmatrix} s_{r,1}(\omega) & & \\ & \ddots & \\ & & s_{r,n_o}(\omega) \end{bmatrix} \begin{bmatrix} w_{r,1}^H \\ \vdots \\ w_{r,n_o}^H \end{bmatrix}$$

$$= WS(\omega)W^H \tag{4.8}$$

where n_o is the total number of outputs. And $s_{r,i}(\omega)$ is the *i*-th most influential mode on $S_{yy}(\omega)$ near ω_r, usually the most influential mode is λ_r. The columns of *W* are linearly independent since they are mode shape vectors corresponding to distinct eigenvalues. Note that *W* does not depend on ω.

The next step is to relate (4.8) to the Singular Value Decomposition (SVD) of $S_{yy}(\omega)$ near ω_r shown as follows.

$$S_{yy}(\omega)|_{\omega near \omega_r} = [u_1(\omega),...,u_{n_o}(\omega)] \begin{bmatrix} \sigma_1(\omega) & & \\ & \ddots & \\ & & \sigma_{n_o}(\omega) \end{bmatrix} \begin{bmatrix} v_1(\omega)^H \\ \vdots \\ v_{n_o}(\omega)^H \end{bmatrix}$$

$$= U(\omega)\Sigma(\omega)V(\omega)^H \tag{4.9}$$

where *U* and *V* are unitary matrices, i.e $UU^H = I$, $VV^H = I$, *I* is identity matrix, *H* denotes complex conjugate transpose. Σ is a diagonal matrix with singular values on the diagonal in decreasing order.

Here $U = V$ because $S_{yy}(\omega)$ is a Hermitian matrix. Then (4.9) becomes

$$S_{YY}(\omega)|_{\omega near \omega_r} = U(\omega)\Sigma(\omega)U(\omega)^H \tag{4.10}$$

Since *U* is unitary, its columns are orthogonal to each other and the rank of U is n_o. The matrix *W* can be spanned by columns of U, i.e. $W = U(\omega)Q(\omega)$. Compare (4.8) and (4.10) above, it is easy to see that

$$\Sigma(\omega) = Q(\omega)S(\omega)Q(\omega)^H \tag{4.11}$$

When the columns of *W* are also orthogonal, *Q* will be a diagonal matrix, thus nonsingular. Then the rank of Σ and *S* will be the same. So the rank of $S_{yy}(\omega)$ evaluated near ω_r, equivalently the number of nonzero singular values, is the same as the number of nonzero terms in $S(\omega)$, i.e. the number of contributing terms.

4.1.1.3) Mode Identification: (4.11) can be written as follows,

$$\Sigma(\omega) = s_{r,1}(\omega)q_1(\omega)q_1^H(\omega) + ... + s_{r,n_o}(\omega)q_{n_o}(\omega)q_{n_o}^H(\omega) \tag{4.12}$$

where q_j is the *j*-th column of *Q*.

Then it follows that

$$\sigma_1(\omega) = s_{r,1}(\omega)q_{11}(\omega)q_{11}^*(\omega) + ... + s_{r,n_o}(\omega)q_{1,n_o}(\omega)q_{1,n_o}^*(\omega)$$

…

$$\sigma_{n_o}(\omega) = s_{r,1}(\omega)q_{n_o,1}(\omega)q_{n_o,1}^*(\omega) + ... + s_{r,n_o}(\omega)q_{n_o,n_o}(\omega)q_{n_o,n_o}^*(\omega) \tag{4.13}$$

where q_{ij} is the *i*-th element in q_j.

In case of single mode contribution near ω_r, $s_{r,2}(\omega),\ldots,s_{r,n_o}(\omega)$ are negligible. Now the first row of (4.13) becomes $\sigma_1(\omega) = s_{r,1}(\omega)q_{11}(\omega)q_{11}^*(\omega)$. In case of multiple modes, if the columns of *W* are also orthogonal, *Q* will be a diagonal matrix. Then, (4.13) becomes

$$\sigma_1(\omega) = s_{r,1}(\omega)q_{11}(\omega)q_{11}^*(\omega)$$

…

$$\sigma_{n_o}(\omega) = s_{r,n_o}(\omega)q_{n_o,n_o}(\omega)q_{n_o,n_o}^*(\omega) \tag{4.14}$$

Furthermore,

$$W^HW = [U(\omega)Q(\omega)]^HU(\omega)Q(\omega) = Q^H(\omega)Q(\omega) \tag{4.15}$$

Thus the element in the first column and first row of W^HW, can be represented as

$$w_{r,1}^Hw_{r,1} = q_1^H(\omega)q_1(\omega) = q_{11}^*(\omega)q_{11}(\omega) + ...q_{n_o,1}^*(\omega)q_{n_o,1}(\omega)$$

$$= q_{11}^{*}(\omega) q_{11}(\omega) \tag{4.16}$$

where $q_{2,1}, \ldots q_{no,1}$ are zero since Q is diagonal.

From (4.14) and (4.16), one arrives

$$\sigma_1(\omega) = s_{r,1}(\omega) w_{r,1}^{H} w_{r,1} \tag{4.17}$$

This means that the largest singular value $\sigma_1(\omega)$ is proportional to $s_{r,1}(\omega)$, which is $s_r(\omega)$ near ω_r. Also, the first left singular vector $u_1(\omega)$ is a normalized version of w_r when the columns of W are orthogonal. Furthermore, the inverse FFT of the largest singular value $\sigma_1(\omega)$ shows the following form

$$\sigma_1(\omega) = \eta s_r(\omega) = \frac{\eta d_r}{\alpha_r^2 + (\omega - \omega_r)^2} = \frac{\eta d_r}{2\alpha_r} \cdot \frac{2\alpha_r}{\alpha_r^2 + (\omega - \omega_r)^2}$$

$$\leftrightarrow f(t) = \frac{\eta d_r}{2\alpha_r} e^{-\alpha_r |t|} e^{j\omega_r t} = B e^{-\alpha_r |t|} e^{j\omega_r t} \tag{4.18}$$

where $\eta = w_r^{H} w_r$ is a scalar, $B = \frac{\eta d_r}{2\alpha_r}$.

For the part t > 0, *f(t)* is in an exponential form as follows

$$f(t) = B e^{(-\alpha_r + j\omega_r)t} = B e^{\lambda_r t} \tag{4.19}$$

The exponential form above is processed by a simple logarithmic decrement technique for damping estimation in [32], [33]. Here, the methods in prony analysis are used [6], since all these methods are based on the exponential sum model. In case of multiple contributing modes near ω_r, if the modes are orthogonal, the SVD process decomposes their impacts into separate singular values. If the modes are non-orthogonal, *Q* is not diagonal and the modes are not completely decomposed. In this case, prony analysis is more appropriate than logarithmic decrement technique, which is suitable for single mode identification only.

4.1.2. Implementation Issues

There are some important technical issues in the actual implementation of FDD. Issues such as verification of basic assumptions and parameter tuning need special attention. Otherwise, the results may lead to incorrect conclusions.

4.1.2.1) Stationarity Test: The basic assumption for all the methods using ambient data is that the ambient measurements are stationary in the normal operating condition and the measurements can be modeled as the outputs from a linear system driven by white noise. This assumption is justified since the highly distributed load variations across the whole system are the only source of inputs for the system during the normal operating condition, and their aggregate effects can be modeled as white noise.

In the implementation of FDD, the first step is to test the stationarity of the measurements before they are further processed. There are many types of non-stationarity, including trend, increasing variance, changing frequency components etc. In this chapter, a simple but powerful method called Reverse Arrangement Test is used [50, Page 105]. It is not able to detect all types of non-stationarity, but works well in most common forms of non-stationarity. First, from a set of observations $x_1, x_2, ...x_N$, define the following function:

$$h_{ij} = \begin{cases} 1 & if\ x_i > x_j \\ 0 & \text{otherwise} \end{cases} \tag{4.20}$$

Then, calculate $M = \sum_{i=1}^{N-1} M_i$, where $M_i = \sum_{j=i+1}^{N} h_{ij}$. M is the total number of reverse arrangement, and its value will fall into some range with some level of significance if the observations are stationary.

4.1.2.2) Estimation of Power Density Spectrum: Power density spectrum estimation is the first step in FDD, thus its accuracy has a great impact on the damping estimation later. Unlike the application of FDD in other fields, the estimation of power density

spectrum becomes a tricky problem for oscillation monitoring. The reason is that the power system is basically a time-varying system and the system condition keeps changing from time to time. Even when the system is operating in a normal state for a long time, it is still desired to use ambient data as short as possible in order to give the system operator sufficient time for preventive control. However, the use of short-time ambient measurements tends to decrease the accuracy of power density spectrum.

The most basic way of spectrum estimation, spectrum by *periodogram* [49, Page 902], is known to be an inconsistent estimate of the true spectrum, and the bias is significant especially when the data is short and Signal Noise Ratio (SNR) is low. The techniques of windowing and moving window average are successfully used to reduce the bias, for example, Welch's method [49] is widely used in FDD for other applications. However, with the same frequency resolution, Welch's method uses several times longer data window, which is not acceptable for our application. In this chapter, the nonparametric method of Multi-Taper Method (MTM) [51] is used. The idea of windowing and averaging in MTM is the same as that in Welch's method, but MTM uses orthogonal data taper, thus it can take average on these orthogonally tapered data to avoid longer time window. The examples in later part of this chapter show that 3 to 5 minutes of data are sufficient for spectrum estimation by Multi-Taper Method.

4.1.2.3) Separation of Modes: As shown in the theoretical part, the largest singular value corresponds to the strongest mode near a poorly damped mode. If the system contains several well-separated poorly-damped modes, there will be several peaks in the plot of largest singular values versus frequencies. Usually this plot of singular values versus frequency is in log scale and called Complex Mode Indication Function (CMIF) plot. Now it is necessary to separate the largest singular values for these peaks and then take inverse FFT. Note that the separation of largest singular values here is different from the SVD process which separate modes into stronger one and weaker ones.

The problem now is to determine the boundary for each mode. Since the first left singular vector is a normalized version of mode shape, the use of Modal Assurance Criterion (MAC) is suggested in [33] to determine whether a specific singular value belongs to a nearby mode or not. MAC provides a measure of degree of similarity between two vectors, it is defined as follows.

$$MAC(\psi_A, \psi_B) = \frac{|\psi_A^H \psi_B|^2}{\psi_A^H \psi_A \cdot \psi_B^H \psi_B} \tag{4.21}$$

In FDD, ψ_A is taken as the left singular vector corresponding to a peak in largest singular value plot. ψ_B is searched in nearby frequency region until the MAC is below some pre-specified value. Any singular vector with an MAC value larger than the pre-specified value is considered to belong to the same mode.

4.1.2.4) Summary of FDD Procedure: The main steps of Frequency domain decomposition is summarized as follows.

Step 1: Test the stationarity of the signals from the PMU measurements. Set a warning flag if the signals do not pass the reverse arrangement test.

Step 2: Estimate the auto and cross power density spectrum by Multi-Taper Method. Form the power spectrum matrix.

Step 3: Within the frequency range of interest, e.g. 0.1 ~ 2.0 Hz for oscillation monitoring, apply SVD to the spectrum matrix evaluated at each frequency line. Plot the largest singular value versus frequency and find the peak in the plot.

Step 4: From the peak of largest singular values, search nearby largest singular values and calculate the MAC value in (4.21). The search terminates when the MAC value is below a pre-specified value.

Step 5: Examine the singular values for a specific mode, check the truncation level as discussed in next section. If severe truncation is observed, set a flag that shows the result is not reliable.

Step 6: Take the singular values from the same mode back to the time domain by inverse FFT. Apply prony analysis to this curve in time domain.

Step 7: Repeat step 4 to step 6 for other peaks in the largest singular values. For automatic mode identification, we can set up a threshold, e.g. 1/4. Only those modes whose peak is larger than 1/4 of the highest peak in CMIF plot are processed by FDD. The number of identified modes is also useful information for oscillation monitoring.

4.2. Test of Frequency Domain Decomposition on Small Linear Systems

4.2.1. Test of FDD for Systems with Different Damping Ratios

In this section, the FDD is tested for simulation data for a known system. First, a system with a poorly damped mode is tested. Usually, a mode with damping ratio less than say 3% is considered poorly damped, while a mode with damping ratio larger than say 10% is well damped. A linear time-invariant (LTI) system with four pairs of poles is created in state space form as in (4.1). The order of matrix *A* is 8, with four modes at 0.25, 0.4, 0.7 and 0.9 Hz respectively. Except that the mode at 0.25 Hz has a damping ratio of 2%, the damping ratios of all other modes are 15%. The system has 2 inputs and 5 outputs and the sampling frequency is 30 Hz. The system matrices are randomly generated as listed in Appendix B. The system is excited by Gaussian white noise for 4 minutes and measurement noises with 20 dB SNR are added to the outputs. The measured data are mean-value-removed and normalized before FDD analysis, but no down-sampling is required. After applying SVD to the spectrum matrix at each frequency line, we get the Complex Mode Indication Function (CMIF) plot, i.e. the plot of singular values in log scale versus frequency. One example is shown in Fig. 4.1. The blue curve at the top of the figure corresponds to the largest singular values and the peak around 0.25 Hz is clearly visible. The second largest singular values are much less than the largest one around 0.25 Hz, which means that the spectrum around the dominant mode is effectively affected by only one mode near 0.25 Hz.

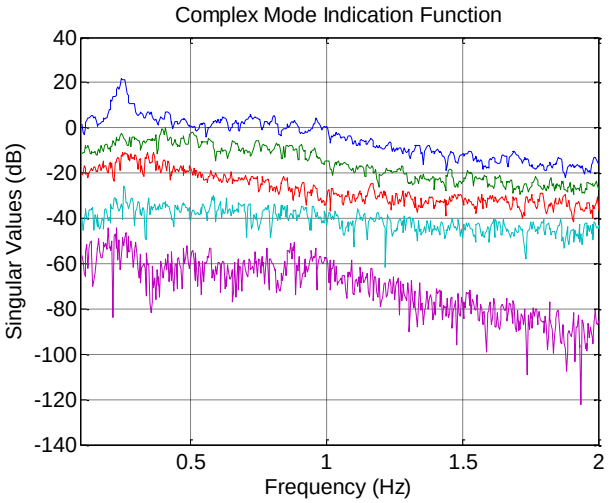

Fig. 4.1. Complex Mode Indication Function (CMIF) for a poorly damped linear system

The test is repeated for 100 times and FDD is performed around the highest peak in CMIF plot. The results are shown in the complex S-plane with y-axis scaled by $1/(2\pi)$ to show the frequency, while x-axis remains unchanged. In Fig. 4.2, the red circles are the true system modes and the blue stars are the identified modes. The mean and standard deviation of 100 identified frequencies are 0.2497 Hz and 0.0024 Hz respectively. The mean and standard deviation of the damping ratios are 2.57% and 1.07% respectively. Compare the results to the true values, and it is concluded that FDD can identify the dominant frequency and damping ratio well under noisy environment.

Next, the damping ratio of the 0.25 Hz mode is changed to 5%. The FDD results for 100 simulation tests are shown in Fig. 4.3. The mean and standard deviation of 100 identified frequencies are 0.2501 Hz and 0.0046 Hz respectively. The mean and standard deviation of the damping ratios are 5.68% and 1.73% respectively. The estimated frequencies are quite accurate and have a small variance. However, the damping ratio estimates have larger variance than the poorly damped case.

In the third case, a reasonably well-damped system is tested. The damping ratio of 0.25 Hz mode is changed to 10% in this case. The FDD results for 100 simulation tests are shown in Fig. 4.4. The mean and standard deviation of 100 identified frequencies are 0.2520 Hz and 0.0094 Hz respectively. The mean and standard deviation of the damping ratios are 8.59% and 2.43% respectively. The biased mean value and a large variance of damping ratio are not surprising because the approximation in developing FDD algorithm is less justified when the actual pole is far away from the imaginary axis. Other tests on well damped systems indicate that FDD is not reasonable for identification of well-damped modes with damping ratios well over +10%. However, the primary focus in real-time oscillation monitoring is the reliable detection of poorly damped modes with damping less than +10% which suits the strengths of the FDD algorithm. Whenever one of the oscillatory modes moves toward the imaginary axis, i.e. when the damping ratio decreases below 10%, the variance of FDD results also decreases, making it possible to capture the problematic mode before it becomes critical.

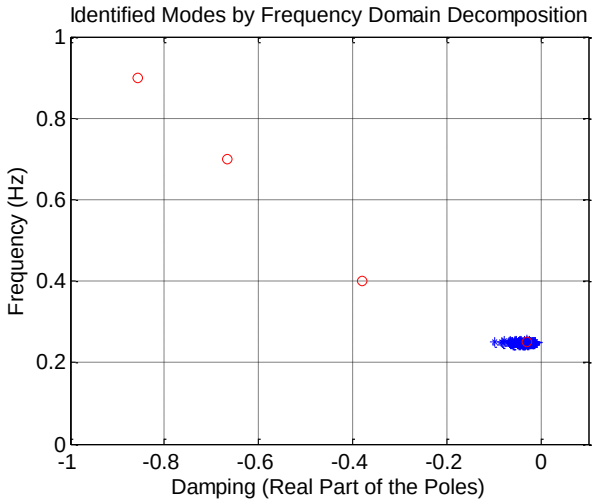

Fig. 4.2. Pole estimates by FDD for a poorly damped LTI system

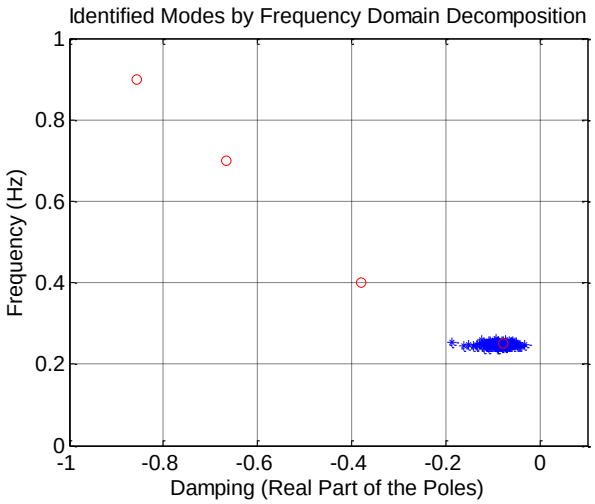

Fig. 4.3. Pole estimates by FDD for a medium damped LTI system

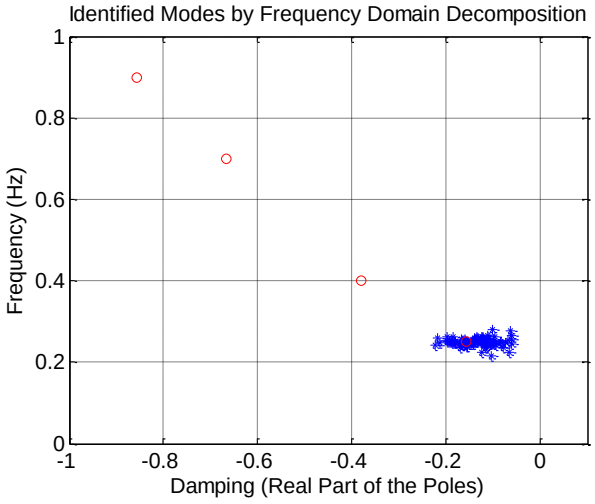

Fig. 4.4. Mode estimates by FDD for a well damped LTI system

Finally, FDD is tested on more systems to show it works for general LTI systems. In the following test, we will randomly change matrices *B*, *C* and *T* as mentioned in Appendix B to create many different test systems. All these systems have the same eigenvalues since matrix Λ remains unchanged. The number of inputs is randomly chosen from 1 to 5, and the number of outputs is randomly chosen form 2 to 5 since FDD only works for more than one output. For each system, excite the system with Gaussian white noise 100 times, and FDD is applied to the outputs using

the same settings as in previous cases. Mean frequency and mean damping ratio from these simulations are recorded for each system. 100 different systems are created for each of the three previous cases with 2%, 5% and 10% damping ratios for the 0.25 Hz mode respectively.

In Table 4.1, we summarize the resulting 100 mean values and standard deviations by their mean value only. Note that the 0.25 Hz mode is not always the most excited one, especially in well damped systems, where the nearby 0.4 Hz mode may be the highest peak in CMIF plot even though it has 15% damping ratio. Whether a specific mode is the most excited one or not depends on not only the damping ratio of the mode, but also the controllability and observability of system depending on matrices *B* and *C* respectively. Even when 0.25 Hz is the highest peak, the damping ratio estimate by FDD can be unreliable due to truncation effect as explained in Section 4.2.4. This phenomenon is more common for well damped systems, where the nearby mode has a larger impact on 0.25 Hz mode. In Table 4.1, we also record the number of times when the 0.25 Hz mode is successfully identified. From Table 4.1, it is clear that FDD works well for general LTI systems, especially when the damping ratio of the most excited mode is low.

TABLE 4.1
TEST OF FDD ON 100 DIFFERENT SYSTEMS

Damping Ratio of 0.25 Hz Mode	0.25Hz Mode Count (Total 10000)	Mean Value of Mean Frequencies (Hz)	Mean of Frequency Standard Deviations (Hz)	Mean Value of Mean Damping Ratios (%)	Mean of Damping Ratio Standard Deviations (%)
2%	9739	0.2504	0.0036	2.69	1.21
5%	9010	0.2522	0.0104	5.70	1.97
10%	7402	0.2553	0.0168	9.27	2.86

The inputs and outputs in the 100 test systems studied in Table 4.1 were chosen randomly as stated earlier. It is interesting that the 0.25 Hz mode is estimated reasonably well for the three damping ratio levels of +2%, +5% and +10% even with

the random choice of inputs and outputs. In practical systems, the estimation results can be relatively made better with a well-designed choice of outputs which show good responses of the oscillatory mode of interest.

4.2.2. Test of FDD for Different Data Lengths

To determine the appropriate data length for real-time application, the performances of FDD for different data lengths are tested on the previous three systems with the *T*, *B* and *C* matrices listed in Appendix B. 100 tests are performed for each data length and the mean and standard deviation of the frequency and damping ratio estimates are compared. The results of the poorly, medium and well damped system are shown in Table 4.2, 4.3 and 4.4 respectively.

From the tables, it is clear that the frequency estimates are all very good for all data lengths tested and longer data lengths tend to provide smaller variance for all three systems. For damping ratio estimation, the standard deviation of the damping ratio estimates usually gets smaller when FDD is applied with longer data length for poorly and medium damped system. However, for the well damped system, increasing data length does not help much for damping ratio estimates. For the poorly and medium damped system, if the data length is too short, like the 2 minute time window length, the damping ratio gets severely biased with large variance. Longer data length tends to have better spectrum estimation and gives smaller variance for damping ratio estimation, but the effect of underestimation is more significant. Also, for the purpose of real-time oscillation monitoring, short data length is desired. For these reasons, 3 to 5 minutes of data are considered appropriate for FDD application in ambient data processing.

TABLE 4.2

EFFECT OF DATA LENGTH ON THE RESULTS OF FDD (2% DAMPING RATIO)

Data Length (minutes)	Mean Frequency (Hz)	Standard Deviation for Frequency (Hz)	Mean Damping Ratio (%)	Standard Deviation for Damping Ratio (%)
2	0.2470	0.0041	5.65	1.21
3	0.2477	0.0029	3.20	0.92
4	0.2497	0.0024	2.57	1.07
5	0.2480	0.0023	2.22	0.81
8	0.2483	0.0017	1.67	0.64
10	0.2480	0.0017	1.46	0.59

TABLE 4.3

EFFECT OF DATA LENGTH ON THE RESULTS OF FDD (5% DAMPING RATIO)

Data Length (minutes)	Mean Frequency (Hz)	Standard Deviation for Frequency (Hz)	Mean Damping Ratio (%)	Standard Deviation for Damping Ratio (%)
2	0.2508	0.0066	7.55	2.07
3	0.2510	0.0051	6.19	1.78
4	0.2501	0.0046	5.68	1.73
5	0.2509	0.0042	5.30	1.80
8	0.2493	0.0028	4.59	1.42
10	0.2494	0.0026	4.39	1.17

TABLE 4.4

EFFECT OF DATA LENGTH ON THE RESULTS OF FDD (10% DAMPING RATIO)

Data Length (minutes)	Mean Frequency (Hz)	Standard Deviation for Frequency (Hz)	Mean Damping Ratio (%)	Standard Deviation for Damping Ratio (%)
2	0.2527	0.0102	9.69	2.01
3	0.2513	0.0098	8.84	2.49
4	0.2520	0.0094	8.59	2.43
5	0.2501	0.0082	8.84	2.10
8	0.2495	0.0078	8.49	2.17
10	0.2498	0.0074	8.06	2.13

4.2.3. Some Features of FDD

As shown previously, FDD is able to give good damping estimation for poorly damped modes. Besides this advantage, FDD also has the following important features.

4.2.3.1) Robustness for Measurement Noise: One of the main advantages of FDD is that it is robust under noisy environment. In the following example, the poorly damped system in Section 4.2.1 is excited by white noise, and four minutes of outputs are contaminated by different levels of measurement noises. 100 tests are performed for each noise level, and the mean and standard deviation of the frequency and damping ratio estimates are compared in Table 4.5. The result in the table shows that FDD gives good estimates even under very noisy environment. The robustness of FDD is due to the relatively low noise energy in the frequency band of 0.1~2 Hz and also the SVD performed in the process. This feature makes FDD very appealing compared to the time domain methods.

TABLE 4.5
EFFECT OF MEASUREMENT NOISE ON FDD (2% DAMPING RATIO)

SNR (dB)	Mean Frequency (Hz)	Standard Deviation for Frequency (Hz)	Mean Damping Ratio (%)	Standard Deviation for Damping Ratio (%)
40	0.2501	0.0024	2.53	0.91
30	0.2500	0.0024	2.86	1.46
20	0.2500	0.0023	2.68	1.06
10	0.2502	0.0025	2.82	1.34
5	0.2499	0.0023	2.54	0.98

4.2.3.2) Mode Shape Identification: As shown in the theoretical part, the singular vector corresponding to the largest singular value near a poorly damped mode is a scaled version of its mode shape. This means that the FDD can also give mode shape estimation. For the poorly damped system in Section 4.2.1, repeat the simulation 30 times and plot the estimated mode shape in Fig. 4.5. The blue solid lines correspond to the normalized true mode shape, and the red dashed lines correspond to the mode shapes estimated by FDD. Note that the SVD process leads to unique left or right singular vectors, up to a multiplication of a unit phase factor $e^{j\phi}$. This multiplication of a unit phase factor $e^{j\phi}$ is in fact a rotation in the complex plane. If rotate the

estimated mode shape in Fig. 4.5, they will match the normalized true mode shape quite accurately as shown in Fig. 4.6, showing the capability of FDD to estimate mode shapes. In practice, only the relative angle differences between mode-shape elements are important and rotation of mode shape is not actually needed.

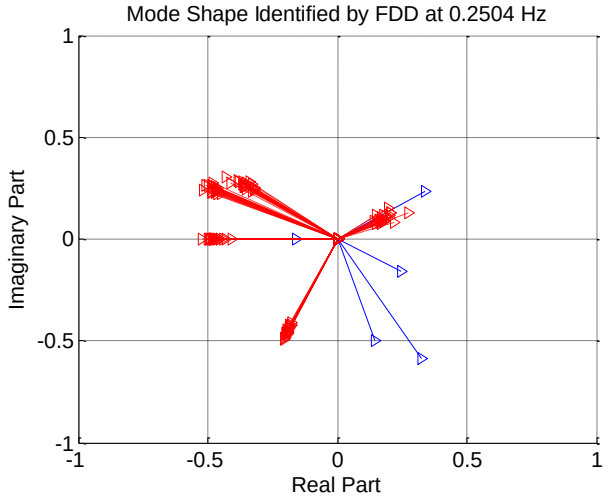

Fig. 4.5. Mode shape identified by FDD for the LTI system

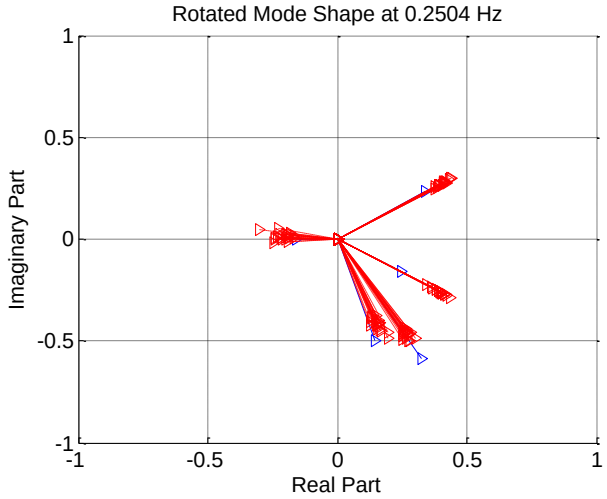

Fig. 4.6. Rotated mode shape identified by FDD for the LTI system

The mode shape information is important in oscillation monitoring in that it provides more information for us to understand the nature of the oscillatory modes of

interest. For instance, mode shape can be used to distinguish whether the mode is a local mode versus inter-area mode, how the different PMUs participate in an oscillatory mode and how the PMUs compare in terms of relative phase angles along the oscillation. Mode shape information is crucial for taking mitigative control actions to improve the damping ratios of problematic modes. Therefore, the capability of FDD to estimate mode shapes is an important advantage over other time domain methods.

4.2.3.3) Correlated Inputs: The basic assumption for ambient data analysis is that the system is excited by load variation modeled by white noises. In the previous tests in this chapter, it is assumed that these white noises at different input locations are completely independent. However, the load variation can be somewhat correlated spatially, for example due to temperature rise in a specific region. In the following test, temporally independent but spatially correlated inputs are applied to the poorly damped system in Section 4.2.1. Now, the correlation matrix between the two inputs is as follows.

$$C = \begin{bmatrix} 1 & \rho \\ \rho & 1 \end{bmatrix}$$

where ρ is correlation coefficient.

TABLE 4.6
EFFECT OF CORRELATED INPUTS ON THE RESULTS OF FDD
(2% DAMPING RATIO)

ρ	Mean Frequency (Hz)	Standard Deviation for Frequency (Hz)	Mean Damping Ratio (%)	Standard Deviation for Damping Ratio (%)
0	0.2501	0.0024	2.51	1.02
0.1000	0.2497	0.0024	2.55	1.11
0.3000	0.2504	0.0022	2.67	1.12
0.5000	0.2503	0.0023	2.49	0.99
0.7000	0.2502	0.0025	2.63	1.12

The result is shown in Table 4.6 and it is seen that FDD is able to handle spatially correlated inputs with reasonable accuracy. Besides spatially correlated inputs, FDD also works for relatively flat input spectrum, thus the basic assumption can be relaxed a little which makes FDD more applicable in real world applications.

4.2.4. Guard against Underestimates

A problem needs special attention when taking singular values of a single mode back to time domain by inverse FFT. The Fourier transform pair in (4.18) is now only a truncated version when MAC value is used to separate individual modes. The singular values whose corresponding left singular vector has a low MAC value with the peak have been discarded, and this leads to a tapering in the frequency domain by a rectangular window. Multiplication of rectangular window in the frequency domain leads to a convolution in the time domain, thus the inverse FFT of truncated singular values no long takes exactly the form in (4.19). An example below is used to clarify this point.

In the following example, a system with a single known mode at 0.3 Hz and 5% damping ratio is tested. In the first case, those singular values less than one half of the peak value are discarded, and the truncated singular values taken back to the time domain by inverse FFT. As shown in Fig. 4.7, the convolution in the time domain leads to an underestimation of the damping ratio. However, if the singular values less than 1/5 of the peak value are discarded, the convolution in time domain has lesser effect and the two curves are almost indistinguishable as shown in Fig. 4.8. In the implementation of FDD, the level for discarding singular values is determined by MAC value. What we can do is to set a warning value, e.g. 1/5, if many singular values larger than 1/5 of the peak value are discarded, the resulting damping ratio from FDD may be underestimated. We put less confidence on these results, or simply discard the result.

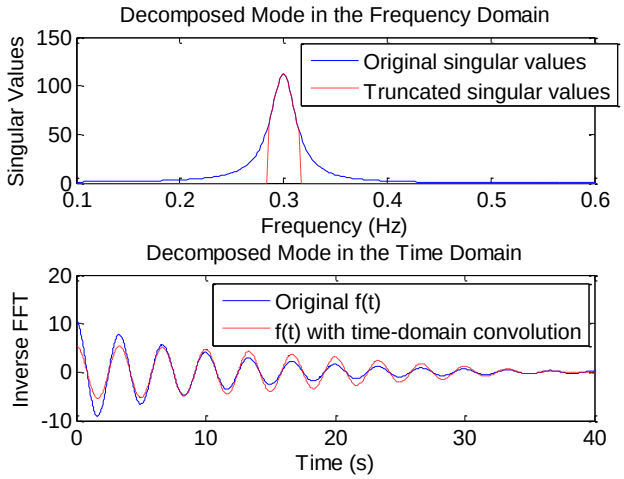

Fig. 4.7. Time domain convolution when singular values less than one half of the peak value are truncated

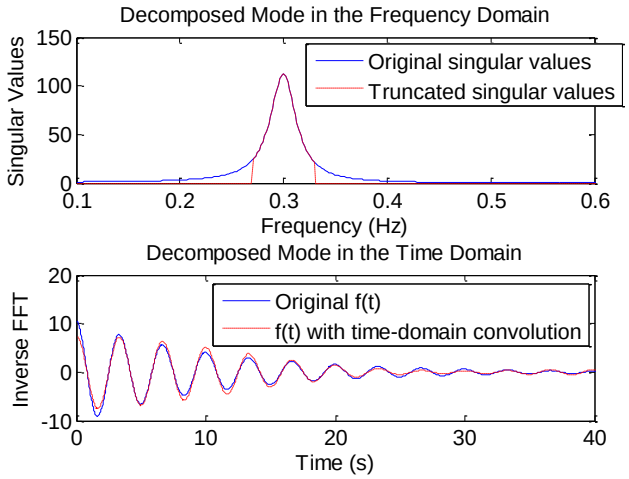

Fig. 4.8. Time domain convolution when singular values less than 1/5 of the peak value are truncated

4.3. Test of Frequency Domain Decomposition on Small Power Systems

FDD has been tested on synthesized linear-time invariant systems in the previous section. In this section, the method of FDD is tested on the simulated responses of a small power system. The two-area four-generator system is taken from [3, 813], and has been used by many researchers. The power-flow condition and the parameters of generators, exciters and PSSs are the same as those in the book. In the following tests, three different cases are created with details shown in Table 4.7. The

power-flow condition remains unchanged for all three cases. The number of PSSs installed has a significant impact on the damping ratios of the inter-area mode, in which the generators G1 and G2 in Area 1 swing against G3 and G4 in Area 2. The frequencies and damping ratios in Table 4.7 are calculated by eigen-analysis using SSAT [46]. These three cases represent a typical poorly damped, medium damped and well damped system respectively.

To simulate random load variations, white Gaussian noise is added to the load at bus 7 using TSAT [47], with the variance being 1% of the total load at that bus. The outputs are recorded at a sampling frequency of 30 Hz. Generator rotor angles at all generators are processed together by FDD. Measurement noise is modeled by white noise passing a low pass filter [20], and the variance of the noise is adjusted so that the Signal Noise Ratio (SNR) is 10 dB. The recorded data are mean-value-removed and normalized before FDD analysis, but no down-sampling is required. The random load simulation is repeated 100 times with 5 minutes data window. One FDD analysis takes an average of 0.76 sec on a laptop with Intel 2GHz CPU and 4GB RAM. The mean and standard deviation of the identified mode frequencies and damping ratios are shown in Table 4.8.

TABLE 4.7
SYSTEM CONDITIONS FOR THREE TEST CASES

Case No.	PSS Installed	Freq. of Inter-area Mode (Hz)	Damping of Inter-area Mode (%)
I	G1	0.6160	2.29
II	G1,G2	0.6123	6.06
III	G1,G2,G3	0.6165	9.21

TABLE 4.8
RESULTS BY FDD FOR THREE TEST CASES USING 5 MINUTES GENERATOR ANGLE DATA

Case	True Freq. (Hz)	Mean Freq. (Hz)	Freq. Std. Dev. (Hz)	True Damping (%)	Mean Damping (%)	Damping Std. Dev. (%)
I	0.6160	0.6162	0.0046	2.29	2.51	0.85
II	0.6123	0.6155	0.0147	6.06	6.18	1.75
III	0.6165	0.6183	0.0244	9.21	7.39	4.26

As shown in Table 4.8, the frequency estimates from FDD are quite accurate for all cases. For damping ratio estimates, the standard deviation grows with increasing system damping. It is not surprising because the approximation in developing FDD algorithm is less justified when the actual pole is far away from the imaginary axis. Fortunately, the primary focus in real-time oscillation monitoring is the reliable detection of poorly damped modes. Whenever one of the oscillatory modes moves toward the imaginary axis, the standard deviation of damping estimates also decreases, making it possible to capture the problematic mode before it becomes critical. Moreover, the standard deviation is very useful in distinguishing a medium damped case as in Case II and a well damped case as in Case III, in which the mean damping ratio is under-estimated. For actual PMU measurements, moving window analysis is used since repeated tests are not possible. Another distinguished feature of FDD is that it is able to estimate mode shape and damping ratios simultaneously. The mode shapes identified in Case I and Case III are compared with theoretical values given by SSAT and shown in Fig. 4.9 and Fig. 4.10 respectively. In the figures, it is clear that the generators G1 and G2 are anti-phase with G3 and G4. This information can be utilized in damping controller design or in other control strategies in real time. Note that mode shape estimates are still good for well damped case as shown in Fig. 4.10.

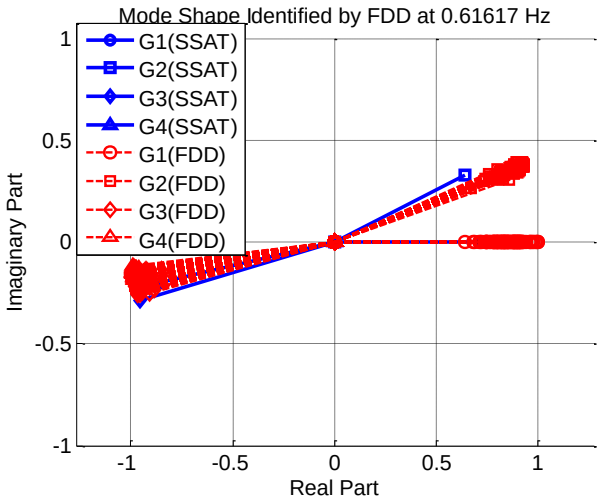

Fig. 4.9. Mode shape estimated by FDD in the two-area system for Case I

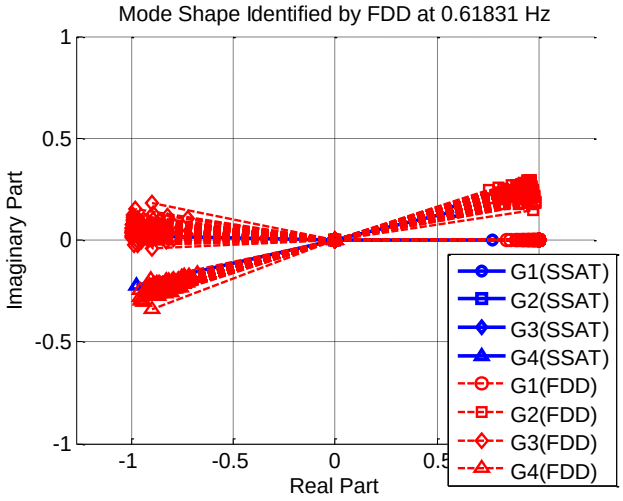

Fig. 4.10. Mode shape estimated by FDD in the two-area system for Case III

Next, FDD is applied to all three cases for different window sizes and compared to two other methods. Here we test FDD on voltage angles at generator buses because they are good approximations of generator rotor angles, which are not directly measured by PMUs. The results are first compared to the ARMA model using the method of modified Yule Walker (YW) [10], [20]. The results are plotted side by side in Fig. 4.11. In the figure, the vertical line is the mean $\pm$ standard deviation versus window size, while the horizontal dash line is the result from eigen-analysis using

SSAT. For each window size, the result from FDD is plotted on the left while YW on the right. The results are also compared to Subspace State Space System Identification (N4SID) [11], [12], [22] as shown in Fig. 4.12. Note that the measurements are low-pass filtered and down-sampled to 5 Hz before applying YW or N4SID. The parameters used are the recommended values (n = 25, m = 10 in YW, n = 20 in N4SID) in [20] and the algorithms are available in DSItoolbox [52] and Matlab System Identification Toolbox [22] respectively.

From the figures, it is seen that FDD gives comparable results as YW and N4SID. All three methods give better estimation when mode damping is low. Frequency estimates are more accurate than damping ratio estimates from all three methods. For damping ratio estimates, the standard deviation grows with increasing system damping, especially in FDD. For well damped system, it is possible for YW or N4SID to reduce the bias and variance by increasing window size and the usual practice is to use 10 minutes or more ambient data [20]. However, increasing window size does not help for FDD because the approximation we made in developing FDD algorithm is less justified when the actual pole is far away from the imaginary axis. After extensive tests, we find that 4 or 5 minutes data window is appropriate for FDD analysis. This data window is updated every 10 sec for moving-window analysis for actual PMU measurements.

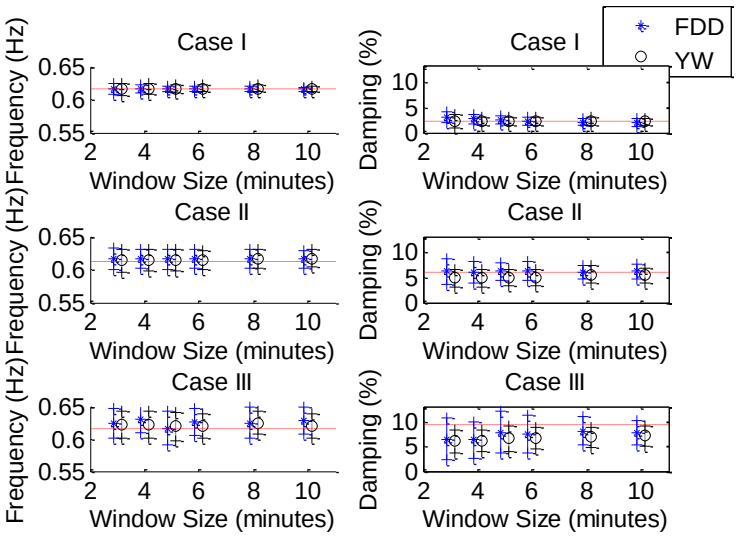

Fig. 4.11. Means and standard deviations of frequency and damping ratio estimates by FDD and YW for all three cases

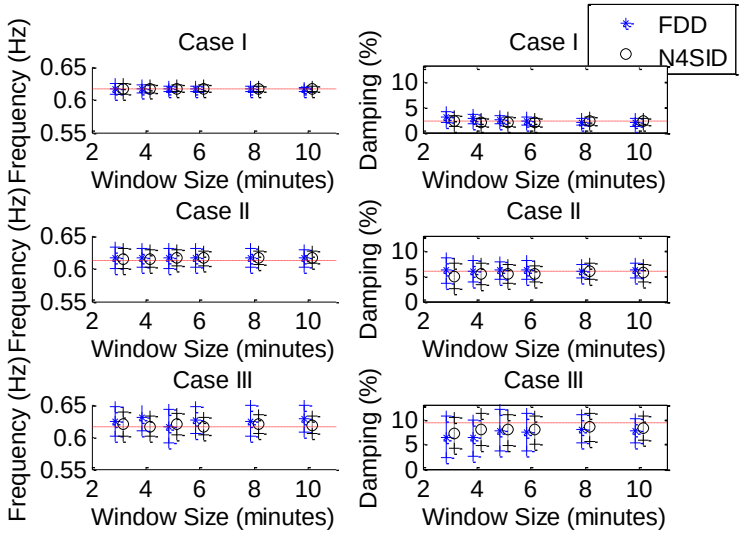

Fig. 4.12. Means and standard deviations of frequency and damping ratio estimates by FDD and N4SID for all three cases

4.4. Case Studies

4.4.1. WECC August 10th 1996 Event

On August 10th 1996, a major blackout occurred in WECC system [1], [2]. At that time, a large amount of power was transmitted from the north to the south. After

some major line-trippings and McNary generator tripping, the western power system experienced a growing oscillation which finally led to a widespread blackout. The active power in one of the major tie-lines from Malin to Round Mountain Line #1 is shown in Fig 4.13 for a brief review of the event. As shown in Fig. 4.13, after the Keeler-Allston 500kV line trips, the system experienced a decaying oscillation. Prony analysis of this signal from 400s to 420s shows a mode at 0.26 Hz with about 2.5% damping ratio. Analysis by other researchers can be found in [48], [53].

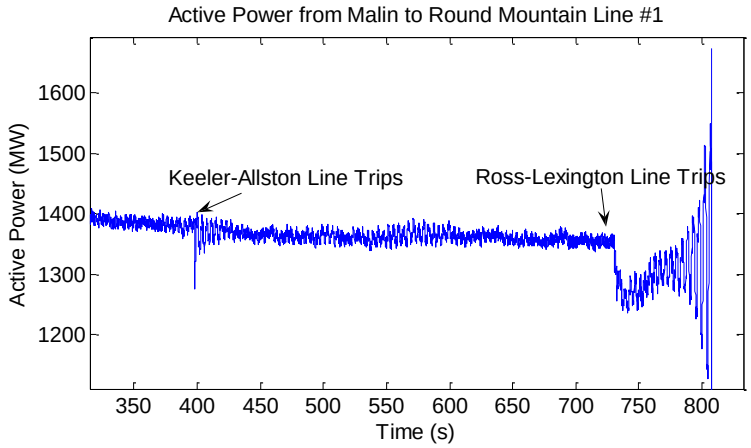

Fig. 4.13. Active power in the tie-line from Malin to Round Mountain line #1 during Aug 10th 1996 blackout

First, FDD is applied to the data before the Keller-Allston line tripping. A total of 12 signals are analyzed simultaneously, including line active powers in Malin-Round Mountain #1, BCH-Custer and LADWP-Celilo etc. The sampling frequency is 20 Hz, and a total of four minutes data are used for each FDD analysis. Moving window analysis is applied and the result is updated every ten seconds. The results are summarized in Table 4.9. To identify the source of the first mode, we check the auto-PSD of each signal and find that the 1 Hz mode only appears in the auto-PSD of McNary generation, indicating that this mode is a local mode involving generators at McNary only. The local nature of the McNary mode can also determined

from the mode shape computed by FDD. Owing to lack of frequency and angle data, illustrations of mode shape computations using FDD are postponed to the next case.

TABLE 4.9
IDENTIFIED MODES FROM FDD ON AUGUST 10TH, 1996

Identified Mode	Mean Frequency (Hz)	Frequency Std. Dev. (Hz)	Mean Damping (%)	Damping Std. Dev. (%)
Highest peak before the 1st line trip	1.0080	0.0016	0.37	0.11
Second highest peak before the 1st line trip	0.2710	0.0012	4.47	1.15
Highest peak after the 1st line trip	0.2510	0.0002	1.60	0.18
Second highest peak after the 1st line trip	0.9701	0.0010	0.25	0.08

The well-known WECC inter-area mode corresponds to the second highest peak in CMIF plot. The result shows that the 0.27 Hz inter-area mode is moderately damped before the tripping of Keeler-Allston line. If the measurement of McNary generation is removed from the signal group and FDD is applied to the remaining measurements, the 0.27 Hz mode will become the highest peak in the CMIF plot, followed by the second highest peak at 0.43 Hz. This result shows the ability of FDD to identify the most excited poorly-damped mode in the current system condition. The above test also validates our signal grouping strategy, i.e. if the signals are grouped in a hierarchical way, the poorly-damped local mode can be identified geographically too.

Next, FDD is applied to the ambient data after the tripping of Keeler-Allston line and before the tripping of Ross-Lexington line. The results are also shown in Table 4.9. Note that the most dominant mode before the tripping of Keller-Allston line is at 1 Hz, and it changed to 0.25 Hz after the line tripping. After the first line tripping, the mode at 1 Hz was already poorly damped; however, it did not become critical. On the other hand, the damping of the 0.25 Hz mode decreased substantially from 4.47% before Keeler-Allston tripping to 1.6% after the line tripping. Even

though the 0.25 Hz mode still had positive damping ratio at around 1.6%, the damping ratio became negative with subsequent tripping of transmission lines and generation in Pacific Northwest [2]. As such, ambient noise analysis by itself could not have detected the emergence of negatively damped 0.25 Hz oscillations during the August 10th, 1996 blackout. However, ambient methods such as FDD illustrated here, could have predicted the proximity of the system to instability by showing extremely low positive damping levels of the 0.25 Hz mode after the Keeler-Allston line tripping.

4.4.2. TVA November 29th 2007 Event

In this case, an example of local mode is shown in the system of Tennessee Valley Authority (TVA). This mode has been observed many times in TVA, and it is found to be related to two generators at Cumberland plant. On Nov 29th 2007, the Power System Stabilizers (PSS) on the generators are off. On 10:13:56 system time, Paradise unit 3 tripped due to a loss-of-excitation condition, the Cumberland machines sensed the trip and responded with a +/- 100MW swing, which damped out in about 15-20 seconds. The plot of voltage angle at Cumberland substation is shown in Fig. 4.14. The sampling frequency is 30 Hz.

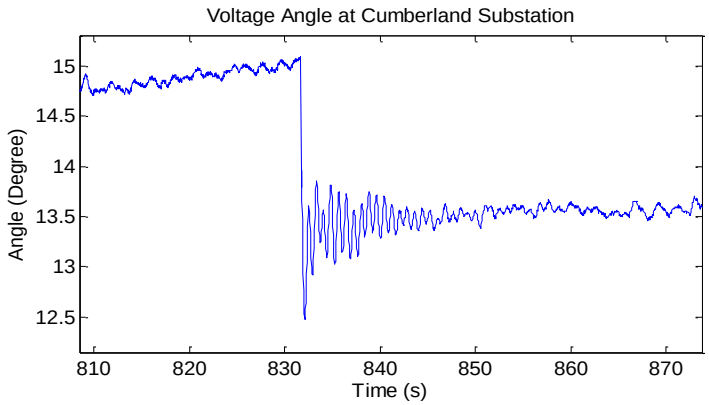

Fig. 4.14. Voltage angle at Cumberland Substation on November 29th, 2007

Prony analysis is applied to all voltage angles from 833 to 843s, where 0 sec corresponds to 10:00 system time. Each signal has its mean removed and been normalized before prony analysis. The result shows a poorly damped local mode at 1.25Hz with 1.5% damping ratio. Prony analysis also gives residue associated with each mode, which is in fact a scaled mode shape [3, Page 710]. The mode shape from prony analysis is shown in Fig. 4.15. Note that the result is normalized, where the largest magnitude of all elements is 1 and the angle at Cumberland is set to be zero. The mode shape shows it is a local mode since voltage angles at Cumberland Substation have much larger magnitudes and also the phase displacements indicate voltage angles at Cumberland Substation swing against the rest of the system.

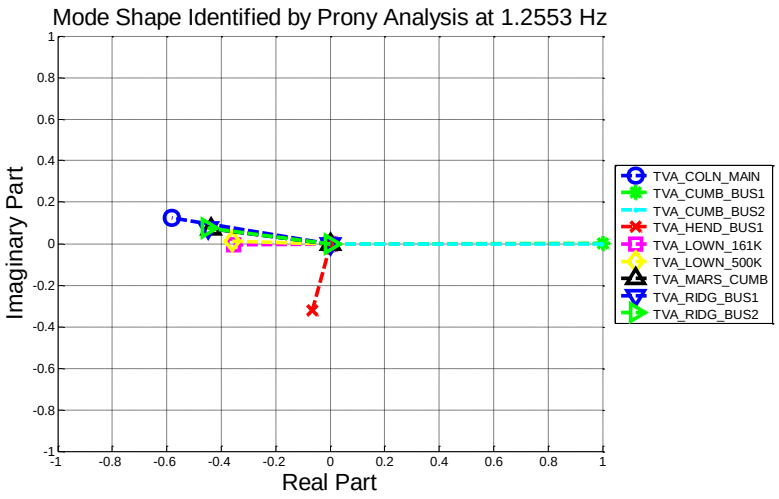

Fig. 4.15. Identified mode shape by prony analysis on Nov 29th 2007 in TVA

Next, FDD is applied to the ambient voltage angles of all available PMUs after the disturbance. Note that the reference angle is the mean value of all voltage angles. FDD analyses use a 4-minute data window and the result is updated every 10 seconds for moving-window analysis. 10 minutes ambient data are tested and the number of total FDD estimates is 37. The moving-window analysis gives the mean frequency of 1.2240 Hz and the mean damping ratio of 1.17%. The standard deviation of frequency estimates is 0.0049 Hz, and the standard deviation of damping ratios is 0.21%.

Finally, the resulting normalized mode shape is shown in Fig. 4.16. The results match well with those obtained from prony analysis.

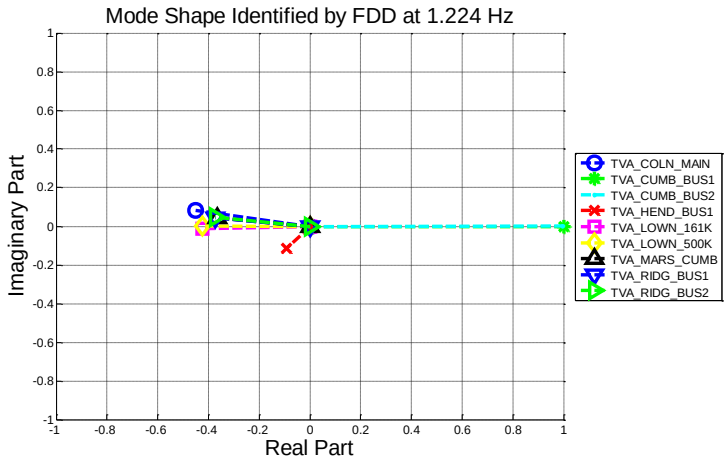

Fig. 4.16. Identified mode shape by FDD on Nov 29th 2007 in TVA

4.4.3. WECC August 22nd 2006 Event

On August 22nd 2006, Bonneville Power Administration (BPA) performed a series of tests to investigate the dynamic performance of the WECC system, including two brake tests, several sinusoidal single mode probing tests and noise probing tests. The results are recorded at 30 Hz in PMUs in various locations throughout the system.

First, prony analysis is applied to two brake tests at 13:10 and 13:15 local time respectively. A total of 15 seconds of bus voltage angles at twelve PMUs are processed. The results using different methods for prony analysis [6] are summarized in Table 4.10. The table clearly shows two major modes of the WECC system: the 0.37 Hz mode called 'Alberta Mode', and the 0.24 Hz mode whose instability led to system blackout in August 10th 1996. Both modes are shown to be well damped.

The normalized mode shapes of both modes are shown in Fig. 4.17 and Fig. 4.18 respectively. The mode in Fig. 4.17 is an inter-area mode because all elements in this mode shape have relative large magnitudes. Moreover, the angles at PMU 9, PMU 10, PMU 8, PMU 4 and PMU 12 form one group, while the angles at the

remaining buses are another group, including PMU 7, PMU 5, etc. These two groups are anti-phase with each other, and the intersection between these two groups is near central-northern Oregon. The mode shape in Fig. 4.18 is also an inter-area mode with high participation on all parts of the system, and the angles at PMU 9, PMU 10, PMU 8, PMU 4 and PMU 12 are still in the same group.

TABLE 4.10

RESULTS OF PRONY ANALYSIS FOR THE BRAKE TESTS ON AUG 22ND 2006

	Analysis Method	Freq. (Hz)	Damp Ratio (%)	Freq. (Hz)	Damp Ratio (%)
Brake Test #1	Prony's Method	0.3756	9.20	0.2457	9.10
	Matrix Pencil	0.3717	8.83	0.2449	9.86
	HTLS	0.3719	8.81	0.2449	9.87
Brake Test #2	Prony's Method	0.3752	10.41	0.2542	9.48
	Matrix Pencil	0.3682	8.51	0.2557	7.45
	HTLS	0.3682	8.50	0.2559	7.44

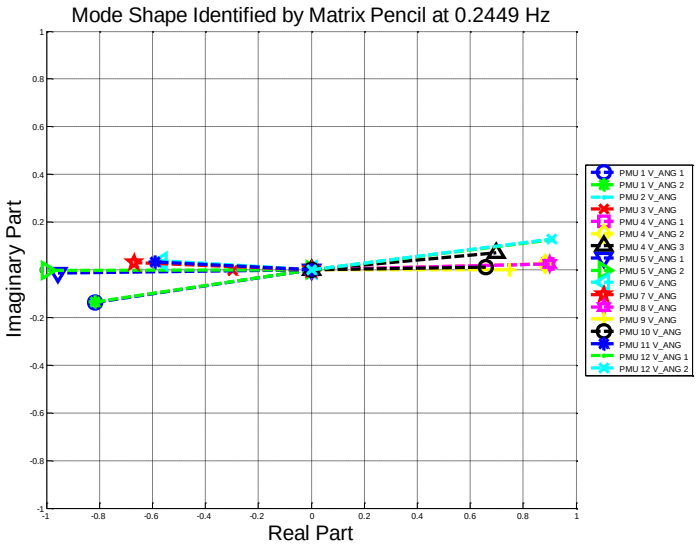

Fig. 4.17. Mode shape of the 0.24 Hz mode by Matrix Pencil Method during the first Chief Joseph Brake test on August 22nd, 2006

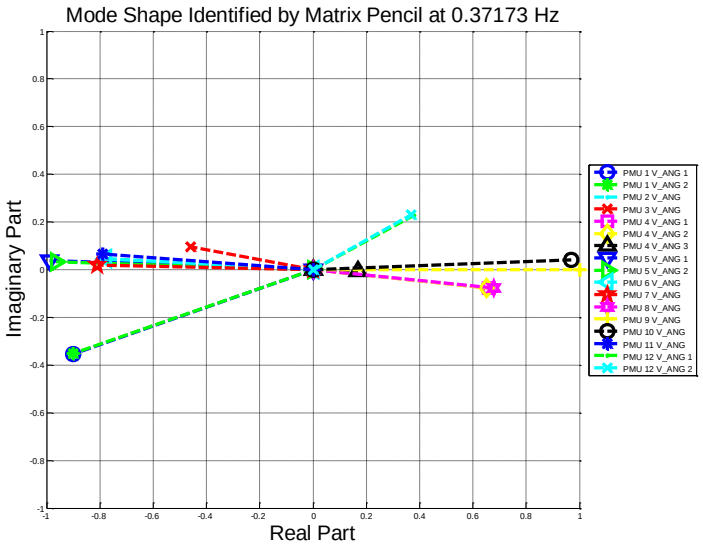

Fig. 4.18. Mode shape of the 0.37 Hz mode by Matrix Pencil Method during the first Chief Joseph Brake test on August 22nd, 2006

Next, FDD is applied to 10 minutes ambient data before the first brake test. The window size for each FDD analysis is 4 minutes, and data window is updated every 10 seconds for moving window analysis, so the total number of FDD performed is 37. The results are summarized in Table 4.11. The results from YW and N4SID are also listed in the table using the same sets of data. For YW and N4SID, the estimation can be improved by using longer data. But for FDD, increasing data window does not help because the approximation in FDD algorithm is less justified when the actual pole is far away from the imaginary axis. Even so, the mean and standard deviation of FDD estimates still clearly indicate that the 0.24 Hz mode is well damped. The damping ratio estimates will be more and more accurate when this mode approaches the imaginary axis. The mean mode shapes by FDD is shown in Fig. 4.19. It is clearly seen that the voltage angles at PMU 9, PMU 10, PMU 8, PMU 4 and PMU 12 are anti-phase with the other PMUs located in the north of the WECC system. The result matches well with the mode shape estimated by prony analysis in Fig. 4.17. FDD is also applied to the 10 minute ambient data after the probing test from 13:21:40 to

13:41:40. The results from FDD, YW and N4SID are also shown in Table 4.11. The resulting mode shape from FDD is shown in Fig. 4.20.

TABLE 4.11
RESULTS OF DIFFERENT METHODS ON AMBIENT AND PROBING TEST DATA ON AUG 22ND 2006

	Analysis Method	Mean Freq. (Hz)	Freq. Std. Dev. (Hz)	Mean Damping (%)	Damping Std. Dev. (%)
Ambient Before Brake Test #1	FDD	0.2302	0.0087	13.13	2.87
	YW	0.2318	0.0126	11.36	2.85
	N4SID	0.2397	0.0105	15.36	3.37
Ambient After Probing Test	FDD	0.2392	0.0061	8.19	2.30
	YW	0.2286	0.0084	8.48	3.21
	N4SID	0.2386	0.0123	12.68	4.48
Probing Test	FDD	0.2268	0.0103	9.98	2.82
	YW	0.2414	0.0060	7.48	2.21
	N4SID	0.2282	0.0148	12.25	5.10

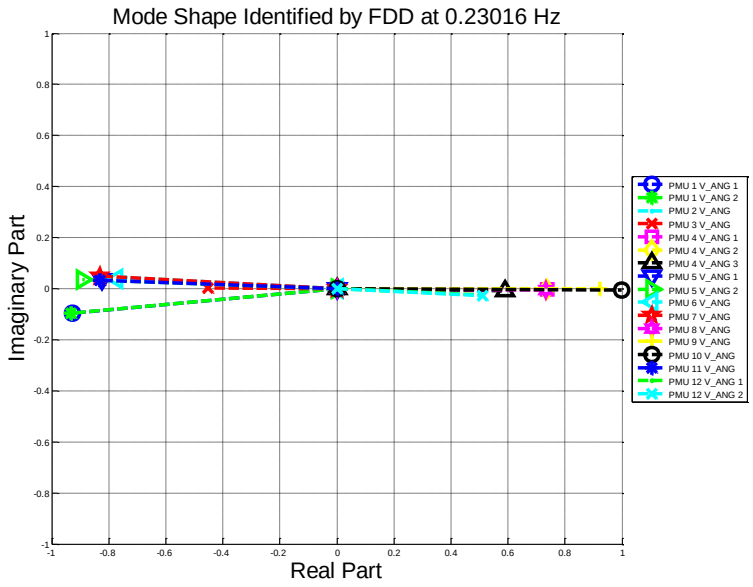

Fig. 4.19. Identified mode shape by FDD before the first brake test on August 22nd 2006

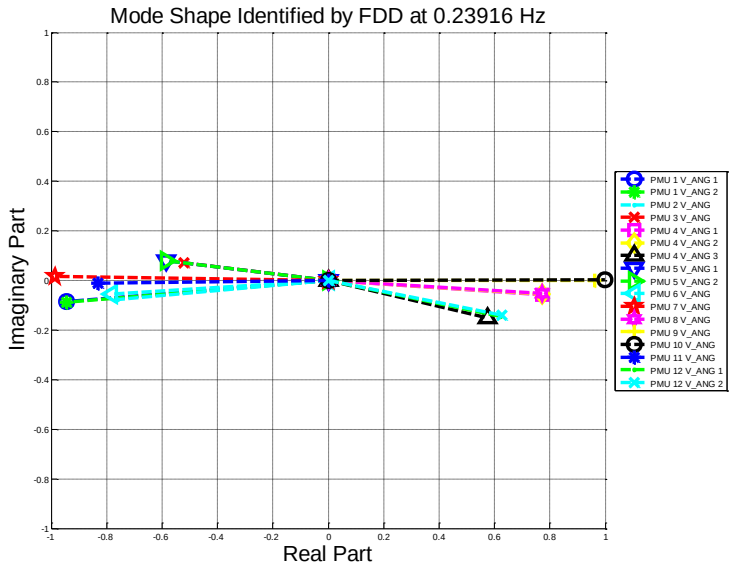

Fig. 4.20. Identified mode shape by FDD after the probing test on August 22nd 2006

Finally, FDD is applied to the noise probing test performed from 13:21:40 to 13:41:40. The low level probing noises were injected into the rectifier side of Pacific HVDC Inter-tie with the bandwidth of 20 Hz. The ambient approaches are valid for noise probing tests because the noise input is independent from load variations across the whole system, thus the basic assumption for ambient condition is still valid. Here, we use the measured outputs only, even though the input is also available. The voltage angles from the same twelve PMUs are used and the parameters for FDD are the same as those in the previous section. Note that the total number of FDD estimates is 97 for 20 min data. The 0.24 Hz mode is successfully estimated 94 times out of the total of 97 and the results are shown in Table 4.11. For noise probing, the 0.37 Hz mode is also excited and identified 33 times. The mean frequency of this mode is 0.3650 Hz with standard deviation of 0.0106 Hz, and the mean damping ratio is 6.99% with standard deviation of 1.57%. The mode shape of the 0.24 Hz and 0.37 Hz mode are plotted in Fig. 4.21 and Fig. 4.22 respectively. The estimated mode shapes match well with the results form prony analysis and previous ambient conditions.

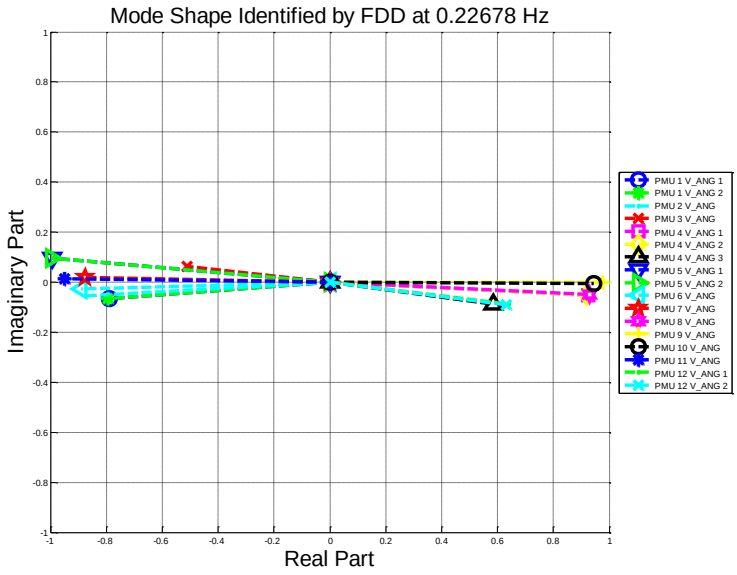

Fig. 4.21. Identified mode shape by FDD during noise probing test on August 22nd 2006 (0.24 Hz mode)

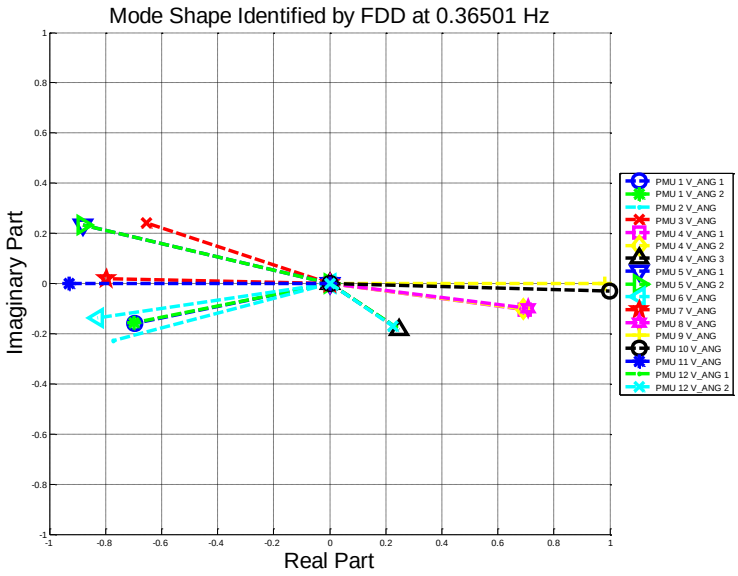

Fig. 4.22. Identified mode shape by FDD during noise probing test on August 22nd 2006 (0.37 Hz mode)

CHAPTER FIVE

CONCLUSIONS

This dissertation presents a complete Oscillation Monitoring System (OMS) based on real-time wide-area measurements from PMUs. This OMS is designed to detect poorly-damped or negatively-damped electromechanical modes in the early stage of an oscillation event, as well as provide warning signals from normal system operating conditions when mode damping becomes insufficient for safe operation of power systems. Depending on different mathematical models of the measured data, different processing algorithms are used. The system disturbance part of the OMS is designed to monitor system events in real-time for the purpose of emergency control, while the ambient part monitors the system without any disturbances for the purpose of preventive control. These two parts are complementary to each other, constituting a complete monitoring system.

Power system responses following system disturbances are in the form of an undamped oscillation or an oscillation back to the old or a new operating point. These responses contain both linear and nonlinear phenomena, especially in the first few cycles immediately following the disturbance. Moreover, presence of noise and switching events in the measurements can upset the accuracy of results. For these reasons, we developed different crosscheck rules to avoid false alarms due to inconsistent estimations. These rules and results have been illustrated on actual PMU recordings.

Ambient data are collected during normal system operations. They are cheap and always available. Ambient data analysis by FDD is well-suited for estimating the frequency, damping ratio, and mode shape of oscillatory electromechanical modes when the respective damping ratios are less than about 10%. FDD also works well for noisy measurements and correlated inputs, and it appears to be useful specifically for

analyzing real-time PMU measurements. Together with the post-disturbance data processing following system events, it provides a powerful framework of an oscillation monitoring system from wide-area PMU measurements.

It is important to remember that power system is actually a high-order time-varying nonlinear system. Only under certain circumstances can it be simplified to linear or time-invariant systems. Ambient condition is reasonably modeled as a linear system because we model all load variations as random small changes around the current operation point. For system response following some events, nonlinearities play an important role in the measured data. Currently in the OMS, prony analysis is combined with moving window analysis and crosscheck rules to deal with these nonlinearity factors. Future research may include algorithms such as Hilbert transform that are used for nonlinear systems.

As for time-varying issue, it is not a major concern for responses following system disturbances because prony analysis uses data of five to twenty seconds each time. However, in the ambient condition, current algorithms including FDD use at least three to five minutes of data. During these three to five minutes, there may be many big or small changes across all the system such that simplification to time invariant system is no longer valid. Thus it is important to apply algorithms that use fewer minutes of data in the future. Future research may include other algorithms from the signal-processing world. Signal processing by artificial neural networks may also be useful.

Oscillation monitoring presented in this dissertation is aimed at small signal stability of power systems. Damping ratios, frequencies and mode shapes obtained from the OMS are important information for damping controller design. There are many research works in controller design based on wide area measurements, but there are still many challenging issues in the real world. Controller design based on wide-area measurements will remain a hot topic in the near future.

REFERENCES

[1] D. N. Kosterev, C. W. Taylor, and W.A. Mittelstadt, "Model validation for the August 10, 1996 WSCC system outage," *IEEE Trans. Power Systems*, vol.14, no.3, pp. 967-979, Aug. 1999.

[2] V. Venkatasubramanian and Y. Li, "Analysis of 1996 western American electric blackouts", *Proc. Bulk Power System Phenomena-Stability and Control*, Venice, Italy, 2004.

[3] P. Kundur, *Power System Stability and Control*. McGraw-Hill, Inc., New York, 1994.

[4] J. Y. Cai, Z. Huang, J. Hauer, and K. Martin. "Current status and experience of WAMS implementation in north america," in *Proc. Transmission and Distribution Conference and Exhibition: Asia and Pacific*, pp. 1-7, 2005.

[5] J. Quintero, "A real-time wide-area control for mitigating small-signal instability in large electric power systems," Ph.D. dissertation, School of EECS, Washington State University, Pullman, WA, May 2005.

[6] G. Liu, J. Quintero, and V. Venkatasubramanian, "Oscillation Monitoring System based on wide area synchrophasors in power systems," *Proc. IREP symposium 2007*. Bulk Power System Dynamics and Control - VII, August 19-24, 2007, Charleston, South Carolina, USA.

[7] A. R. Messina and V. Vittal, "Nonlinear, non-stationary analysis of interarea oscillations via Hilbert spectral analysis," *IEEE Trans. Power Systems*, pp. 1234-1241, Aug. 2006.

[8] G. Ledwich and E. Palmer. "Modal estimates from normal operation of power systems," in *Proc. 2000 Power Engineering Society Winter Meeting*, pp. 1527-1531

[9] J. W. Pierre, D. J. Trudnowski, and M. K. Donnelly, "Initial results in electromechanical mode identification from ambient data," *IEEE Trans. Power Systems*, vol. 12, pp. 1245-1251, Aug. 1997.

[10] R. W. Wies, J. W. Pierre, and D. J. Trudnowski, "Use of ARMA block processing for estimating stationary low-frequency electromechanical modes of power systems," *IEEE Trans. Power Systems*, vol. 18, pp. 167-173, Feb. 2003.

[11] N. Zhou, J. W. Pierre, and R. W. Wies, "Estimation of low-frequency electromechanical modes of power systems from ambient measurements using a subspace method," *35th North American Power Symposium*, Rolla, Missouri, Oct 2003.

[12] H. Ghasemi, C. Canizares, and A. Moshref, "Oscillatory stability limit prediction using stochastic subspace identification," *IEEE Trans. Power Systems*, vol. 21, pp. 736-745, May 2006.

[13] P. Korba, M. Larsson, and C. Rehtanz, "Detection of oscillations in power systems using Kalman filtering techniques," in *Proc. 2003 IEEE Conference on Control Applications*, pp. 183-88.

[14] R. W. Wies, J. W. Pierre and D. J. Trudnowski, “Use of least mean squares (LMS) adaptive filtering technique for estimating low-frequency electromechanical modes in power systems,” *Power Engineering Society General Meeting*, vol.2 , pp. 1863-1870, 2004.

[15] N. Zhou, J. W. Pierre, D. J. Trudnowski, and R. T. Guttromson, "Robust RLS methods for online estimation of power system electromechanical modes," *IEEE Trans. Power Systems*, vol. 22, pp. 1240-1249, Aug. 2007.

[16] N. Zhou, D. J. Trudnowski, J. W. Pierre and W. A. Mittelstadt, "Electromechanical mode online estimation using regularized robust RLS methods," *IEEE Trans. Power Systems*, vol. 23, pp. 1670-1680, Nov. 2008.

[17] D. J. Trudnowski and J. W. Pierre, "Overview of algorithms for estimating swing modes from measured responses", presented at the IEEE Power & Energy Society General Meeting, Calgary, Alberta, Canada, 2009.

[18] H. Hiraiwa, H. Saitoh,, E. Tsukada, K. Minazawa, and J. Toyoda, "System-response-based eigenvalue estimation for on-line assessment of power system stability," *Proc. 2004 IEEE International Conference on Electric Utility Deregulation, Restructuring and Power Technologies*. April 2004, pp. 366-371

[19] T. Hiyama and N. Suzuki, "Real time modal analysis of power system oscillations," *Proc. IEEE International Symposium on Circuits and Systems*, 2000, Geneva, pp. 225-228.

[20] D. J. Trudnowski, J. W. Pierre, N. Zhou, J. F. Hauer and M. Parashar, "Performance of three mode-meter block-processing algorithms for automated dynamic stability assessment," *IEEE Trans. Power Systems*, vol. 23, pp. 680-690, May 2008.

[21] N. Kakimoto, M. Sugumi, T. Makino, and K. Tomiyama, "Monitoring of interarea oscillation mode by synchronized phasor measurement," *IEEE Trans. Power Systems*, vol. 21, pp. 260-268, Feb. 2006.

[22] L. Ljung, *System Identification Toolbox 7, User's Guide*, The MathWorks, Inc., Natick, MA, USA, March 2008.

[23] D. J. Trudnowski, "Estimating electromechanical mode shape from synchrophasor measurements," *IEEE Trans. Power Systems*, vol. 23, pp. 1188 - 1195, Aug. 2008.

[24] M. Banejad and G. Ledwich, “Correlation based mode shape determination of a power system,” in *Proc. 2002 IEEE Int. Conf. Acoustics, Speech, and Signal Processing*, vol. 4, pp. 3832-3835

[25] N. Zhou, Z. Huang, L. Dosiek, D. Trudnowski and J. W. Pierre, "Electromechanical mode shape estimation based on transfer function

identification using PMU measurements", presented at the IEEE Power & Energy Society General Meeting, Calgary, Alberta, Canada, 2009.

[26] L. Dosiek, J. W. Pierre, D. J. Trudnowski and N. Zhou, "A channel matching approach for estimating electromechanical mode shape and coherence", presented at the IEEE Power & Energy Society General Meeting, Calgary, Alberta, Canada, 2009.

[27] G. Liu and V. Venkatasubramanian, "Oscillation monitoring from ambient PMU measurements by Frequency Domain Decomposition," *Proc. IEEE International Symposium on Circuits and Systems*, Seattle, WA, May 2008, pp. 2821-2824.

[28] G. Liu, V. Venkatasubramanian and J. R. Carroll, "Oscillation monitoring system using synchrophasors," *Power & Energy Society General Meeting*, July 2009.

[29] V. Venkatasubramanian and J. R. Carroll, "Oscillation Monitoring System at TVA", presentation at NASPI meeting, New Orleans, LA, Mar. 2008, http://www.naspi.org/meetings/workgroup/2008_march/session_one/tva_oscillation_monitoring_venkatasubramanian.pdf

[30] C.Y. Shih, Y.G. Tsuei, R.J. Allemang, and D.L. Brown. "Complex mode indication function and its applications to spatial domain parameter estimation," *Mechanical Systems and Signal Processing*, vol. 2, pp. 367-377. Oct. 1988.

[31] R. Brincker, L. Zhang and P. Andersen. "Modal identification from ambient responses using Frequency Domain Decomposition," *Proc. the 18th International Modal Analysis conference (IMAC)*, San Antonio, Texas, February 7-10, 2000

[32] R. Brincker, C. E. Ventura, and P. Andersen, "Damping estimation by Frequency Domain Decomposition," *Proc. the 19th International Modal Analysis Conference (IMAC)*, Kissimmee, Florida, 2001. pp. 698-703.

[33] T. Wang and L. Zhang. "Frequency and Spatial Domain Decomposition for operational modal analysis and its application," *Acta Aeronautica et Astronautica Sinica*., vol. 27, pp. 62-66. Jan. 2006

[34] *IEEE Standard for Synchrophasors for Power Systems*, IEEE Std C37.118-2005, 2006.

[35] G. R. B. Prony, "Essai experimental et analytique sur les lois de la dilatalrlite de fluids elastiques et sur cells de la vapeur de l'alcool, à différents tempoeratures," *Journal de l'Ecole Polytechnique (París),* vol. 1, pp. 24-76, 1795.

[36] J. F. Hauer, C. J. Demeure, and L. L. Scharf, "Initial results in Prony analysis of power system response signals," *IEEE Trans. Power Systems*, vol. 5, pp. 80-89, Feb. 1990.

[37] D. J. Trudnowski, J. R. Smith, T. A. Short, and D. A. Pierre, "An application of Prony methods in PSS design for multi-machine systems," *IEEE Trans. Power Systems*, vol. 6, pp. 118-126, Feb. 1991.

[38] D. J. Trudnowski., J. M. Johnson, and J. F. Hauer, "Making prony analysis more accurate using multiple signals," *IEEE Trans. Power Systems*, vol. 14, pp. 226-231, Feb. 1999.

[39] T. K. Sarkar and O. Pereira, "Using the matrix pencil method to estimate the parameters of a sum of complex exponentials," *IEEE Antennas and Propagation Magazine*, vol. 37, pp. 48-55, Feb. 1995.

[40] Y. Hua and T. K. Sarkar, "On SVD for estimating generalized eigenvalues of singular matrix pencil in noise," *IEEE Trans. Signal Processing*, vol. 39, pp. 892-900, Apr. 1991.

[41] Y. Hua and T. K. Sarkar, "Matrix pencil method for estimating parameters of exponentially damped/undamped sinusoids in noise," *IEEE Trans. Acoustics, Speech, and Signal Processing*, vol. 38, pp. 814-824, May 1990.

[42] M. L. Crow and A. Singh, "The matrix pencil for power system modal extraction," *IEEE Trans. Power Systems*, vol. 20, pp. 501-502, Feb. 2005.

[43] J. M. Papy, L. D. Lathauwer, and S. V. Huffel, "Common pole estimation in multi-channel exponential data modeling," *Signal Processing*, vol. 86, pp. 846-858, 2006.

[44] L. Vanhamme and S. V. Huffel, "Multichannel quantification of biomedical magnetic resonance spectroscopy signals," *Advanced Signal Processing Algorithms, Architectures and Implementations VIII, Proceedings of SPIE*, vol. 3461, pp. 237- 245, 1998.

[45] D. J. Trudnowski, and J. E. Dagle, "Effects of generator and static-load nonlinearities on electromechanical oscillations," *IEEE Trans. Power Systems*, vol. 12, pp. 1283-1289, Aug. 1997.

[46] *Small Signal Analysis Tool (SSAT), User's Manual*, Powertech Labs Inc., Surrey, BC, Canada, 2002.

[47] *Transient Security Assessment Tool (TSAT), User's Manual*, Powertech. Labs Inc., Surrey, BC, Canada, 2002.

[48] J. F. Hauer, M. J. Beshir, and W. Mittelstadt, "Dynamic performance validation in the western power system," Presented on behalf of the WSCC Performance Validation Task Force at the APEx 2000 in Kananaskis, Alberta, Oct. 2000.

[49] J. G. Proakis and D. G. Manolakis. *Digital Signal Processing: Principles, Algorithms, and Applications*. 1996, Prentice-Hall, Inc. Upper Saddle River, NJ, USA.

[50] J. S. Bendat and A.G. Piersol. *Random Data Analysis and Measurement Procedures*. John Wiley & Sons, Inc, New York, NY, USA. 2000, 3rd ed.

[51] D. J. Thomson, "Spectrum estimation and harmonic analysis," *Proceedings of the IEEE*, vol. 70, pp. 1055-1096, Sep. 1982.

[52] J. M. Johnson and D. J. Trudnowski, *DSItools Ringdown Analysis Tool, Users' Manual*, Battelle Memorial Institute.

[53] J. F. Hauer, D. J. Trudnowski, and J. G. DeSteese, "A perspective on WAMS analysis tools for tracking of oscillatory dynamics," in *Proc. 2007 IEEE Power Engineering Society General Meeting*, pp. 1-10.

APPENDIX A

When the inputs to the linear system are white noise, the power density spectrum matrix of outputs is calculated as follows.

$$S_{yy}(\omega) = H(j\omega)\cdot F\cdot H(j\omega)^H$$

$$= \left[\sum_{i=1}^{n}\frac{R_i}{j\omega-\lambda_i}\right]\cdot F\cdot\left[\sum_{k=1}^{n}\frac{R_k}{j\omega-\lambda_k}\right]^H$$

$$= \sum_{i=1}^{n}\left[\frac{R_i F}{j\omega-\lambda_i}\sum_{k=1}^{n}\frac{R_k^H}{-j\omega-\lambda_k^*}\right]$$

$$= \sum_{i=1}^{n}\left[R_i F\sum_{k=1}^{n}\frac{-R_k^H}{(j\omega-\lambda_i)(j\omega+\lambda_k^*)}\right] \qquad \text{(A.1)}$$

Apply partial fraction decomposition to (A.1), then $S_{yy}(\omega)$ can be written as

$$\sum_{i=1}^{n}\left[R_i F\sum_{k=1}^{n}\left(\frac{\frac{-R_k^H}{\lambda_i+\lambda_k^*}}{j\omega-\lambda_i}+\frac{\frac{R_k^H}{\lambda_k^*+\lambda_i}}{j\omega+\lambda_k^*}\right)\right]$$

$$= \sum_{i=1}^{n}\frac{R_i F\sum_{k=1}^{n}\frac{-R_k^H}{\lambda_i+\lambda_k^*}}{j\omega-\lambda_i}+\sum_{i=1}^{n}\sum_{k=1}^{n}\frac{\frac{R_i F R_k^H}{\lambda_k^*+\lambda_i}}{j\omega+\lambda_k^*} \qquad \text{(A.2)}$$

Change the summation order of the second term, and use a change of variables, the second term in (A.2) now becomes $\sum_{i=1}^{n}\sum_{k=1}^{n}\frac{\frac{R_k F R_i^H}{\lambda_i^*+\lambda_k}}{j\omega+\lambda_i^*}$. Thus,

$$S_{yy}(\omega) = \sum_{i=1}^{n}\left[\frac{R_i F\sum_{k=1}^{n}\frac{-R_k^H}{\lambda_i+\lambda_k^*}}{j\omega-\lambda_i}+\sum_{k=1}^{n}\frac{\frac{R_k F R_i^H}{\lambda_i^*+\lambda_k}}{j\omega+\lambda_i^*}\right]$$

$$= \sum_{i=1}^{n}\left[\frac{R_i F\sum_{k=1}^{n}\frac{-R_k^H}{\lambda_i+\lambda_k^*}}{j\omega-\lambda_i}+\frac{(\sum_{k=1}^{n}\frac{R_k}{\lambda_i^*+\lambda_k})F R_i^H}{j\omega+\lambda_i^*}\right] \qquad \text{(A.3)}$$

Denote the numerator of the first term in (A.3) as A_i. The numerator of the second term turns out to be $-A_i^H$. Then $S_{yy}(\omega)$ can be expressed as follows.

$$S_{yy}(\omega) = \sum_{i=1}^{n} \left[\frac{A_i}{j\omega - \lambda_i} - \frac{A_i^H}{j\omega + \lambda_i^*} \right] \tag{A.4}$$

APPENDIX B

The LTI system matrices in Section 4.2 are created as follows. Given a pair of eigenvalues $\lambda_i = -\alpha_i \pm j\omega_i$, form a 2×2 matrix $\Lambda_i = \begin{bmatrix} -\alpha_i & -\omega_i \\ \omega_i & -\alpha_i \end{bmatrix}$ for this mode. Then form a block diagonal matrix Λ by placing all Λ_i's on the diagonal. After a similarity transformation $A = T\Lambda T^{-1}$, the system matrix A will have exactly the same eigenvalues as specified. For example, in the system we tested in Section 4.2.1, the four pairs of eigenvalues are at 0.25, 0.4, 0.7 and 0.9 Hz, with damping ratio at 2%, 15%, 15% and 15% respectively, then

$$\Lambda = \begin{bmatrix} -0.0314 & -1.5708 & 0 & 0 & 0 & 0 & 0 & 0 \\ 1.5708 & -0.0314 & 0 & 0 & 0 & 0 & 0 & 0 \\ 0 & 0 & -0.3813 & -2.5133 & 0 & 0 & 0 & 0 \\ 0 & 0 & 2.5133 & -0.3813 & 0 & 0 & 0 & 0 \\ 0 & 0 & 0 & 0 & -0.6673 & -4.3982 & 0 & 0 \\ 0 & 0 & 0 & 0 & 4.3982 & -0.6673 & 0 & 0 \\ 0 & 0 & 0 & 0 & 0 & 0 & -0.8579 & -5.6549 \\ 0 & 0 & 0 & 0 & 0 & 0 & 5.6549 & -0.8579 \end{bmatrix}$$

The system matrix A is then calculated by $A = T\Lambda T^{-1}$, where T is randomly generated and remains the same throughout Section III as shown below.

$$T = \begin{bmatrix} -0.6397 & 2.2879 & 0.4195 & 1.2954 & -0.8507 & -0.1733 & -1.0571 & -1.8112 \\ -0.3406 & -1.5785 & 1.5725 & -0.6758 & 0.2319 & 0.5441 & 0.2647 & 0.5483 \\ 0.1071 & -1.0151 & 0.1343 & -0.0692 & 1.0090 & 0.2324 & 0.7395 & -1.1047 \\ 0.3991 & -0.7025 & -0.8004 & 0.0023 & -1.5566 & -0.9459 & 0.7033 & -0.0105 \\ -0.8997 & 0.2034 & 0.4565 & 1.6502 & -0.7338 & -1.2531 & 0.4449 & -0.0098 \\ -1.0721 & 1.9230 & -1.7455 & -1.8737 & 0.0632 & 0.1711 & 0.4426 & -0.0155 \\ 1.2374 & 1.0380 & 0.1062 & 0.1294 & 0.1893 & 1.1157 & -0.7342 & 0.8921 \\ 2.0924 & 0.8661 & -1.2261 & 0.2063 & 0.1435 & -0.2157 & -0.5591 & 0.6928 \end{bmatrix}$$

The matrices B, C in (4.1) are also generated randomly as follows. For other systems in Section 4.2, the only modification is made on Λ_i to change the damping ratio of a specific mode.

$$B = \begin{bmatrix} -1.2264 & -0.6979 \\ -0.2657 & -2.4476 \\ -0.0121 & 0.2493 \\ -0.9393 & -1.7079 \\ -1.1177 & 0.5074 \\ -0.8453 & -0.6638 \\ 1.6256 & -1.9224 \\ 0.8401 & 1.2831 \end{bmatrix}$$

$$C = \begin{bmatrix} -0.0503 & -0.6467 & -0.1988 & -0.3905 & 0.6531 & 0.5375 & -1.2928 & 0.4272 \\ 0.7545 & -0.0280 & -0.9372 & 0.4031 & 1.4962 & -0.4181 & -1.3347 & -0.5944 \\ 0.4666 & -0.5162 & 0.4280 & -0.3818 & 0.8755 & 0.0169 & 0.6588 & 0.6327 \\ 0.2806 & 0.9963 & -1.9581 & -1.3605 & 0.1146 & 0.6049 & -1.1407 & -0.8815 \\ -1.0731 & -0.7952 & -1.3490 & 2.0034 & 1.4633 & -0.2116 & 0.3652 & -0.3046 \end{bmatrix}$$